Diffusion Self-Ignition of Hydrogen in Air

Victor Golub
Associated Institute for High Temperatures,
Russian Academy of Sciences
13/19 Izhorskaya st., Moscow, 125412, Russia
E-mail: *golub@ihed.ras.ru*

Motivation

Ignition source	Hydrogen incidents	
	Number	%
Collision	2	2.5
Flame	3	3.7
Hot Surface	2	2.5
Electric	2	2.5
Friction Spark	2	2.5
Non identified	70	86.3
Non-ignition	0	0
Total	81	100.0

Frequency of occurrence of ignition sources (G.R. Astbury, S.J. Hawksworth , 2005).

State of problem

Gas escape from reservoirs and pipelines can lead to the ignition of hydrogen followed by the explosion of fuel-air mixture

This problem is of current importance today because of hydrogen energy development compelled to ensure storage safety of high-pressure reservoirs.

Industry is developing

high pressure composite hydrogen tank

that stores hydrogen at 10,000 psi

(700 Bar)!!!!

QUANTUM Technologies WorldWide, Inc

Explosive questions:

- What is impulse hydrogen jet structure when there is a leak in the tank or during a safety-valve operation?

- Can the cold hydrogen jet ignite by itself or not?

Necessary and sufficient condition for ignition of combustible mixture is:

The temperature have to be higher than ignition temperature during the time longer than ignition time.

Background of the diffusion ignition

The phenomenon of diffusion ignition has been postulated by Wolański and Wójcicki (1973), who demonstrated that ignition occurred when high pressure hydrogen was admitted to shock tube filled with air or oxygen. They found that ignition could be achieved even if the temperature was below the autoignition temperature of the hydrogen and occurs as a result of sharp temperature jump of the combustible mixture created by diffusion on the contact surface of hydrogen with oxidizer heated by the primary shock wave.

Contents

- Introduction
- Hydrogen impulse jet self-ignition in semi-confined space
  - Experimental investigation of impulse jet
  - Numerical simulation of impulse jet
  - Numerical simulation of self-ignition
  - Conclusions
- Hydrogen self-ignition in tubes
  - Experimental investigation of self-ignition in tubes
  - Numerical simulation of self-ignition in tubes
  - Conclusions

Over the last century, there have been reports of high pressure hydrogen leaks igniting for no apparent reasons

Several ignition mechanisms have been proposed:

- Reverse Joule-Thomson effect
- Electrostatic charge generation
- Diffusion ignition
- Sudden adiabatic compression
- Hot surface ignition

Astbury G.R., & Hawksworth S.J. (2005).

Hydrogen impulse jet self-ignition in semi-confined space

Experimental setup photo

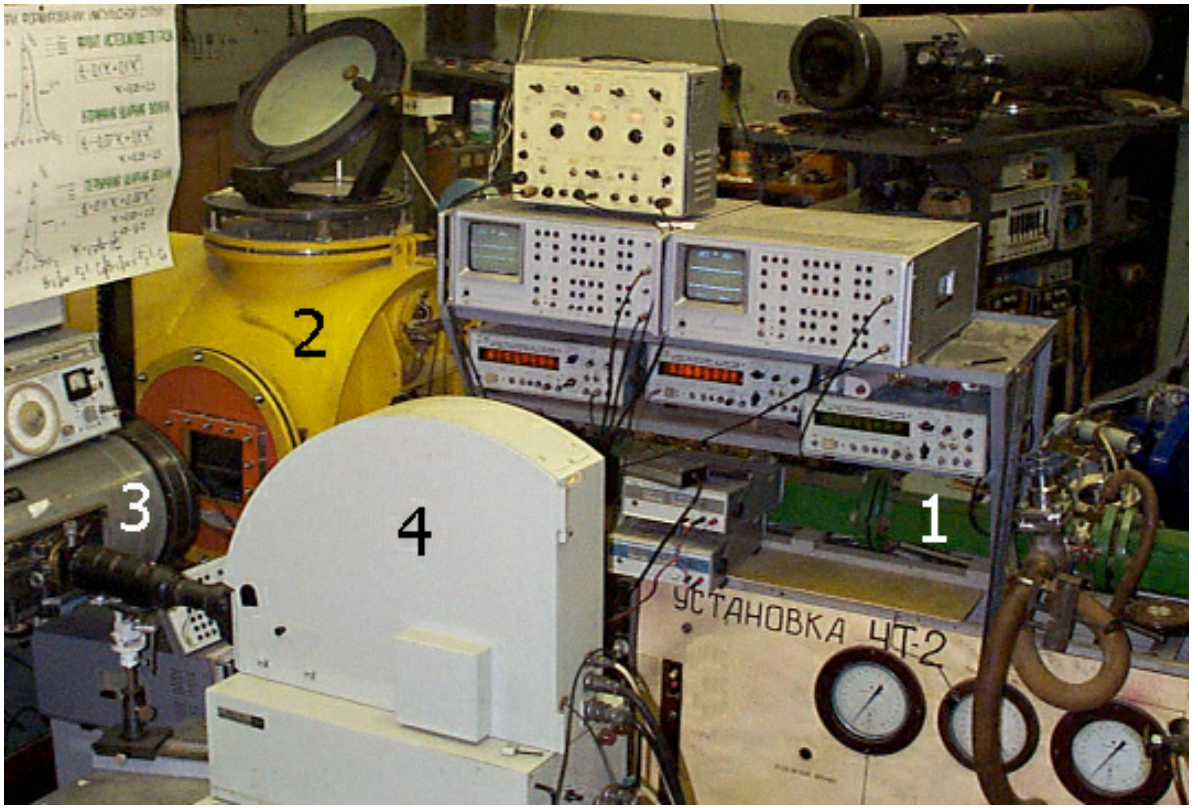

1 – Detonation/shock tube
2 – Receiver/vacuum chamber
3 – IAB-451 schlieren device
4 – High-speed photo-registration camera

Schlieren photographs of the impulse jet

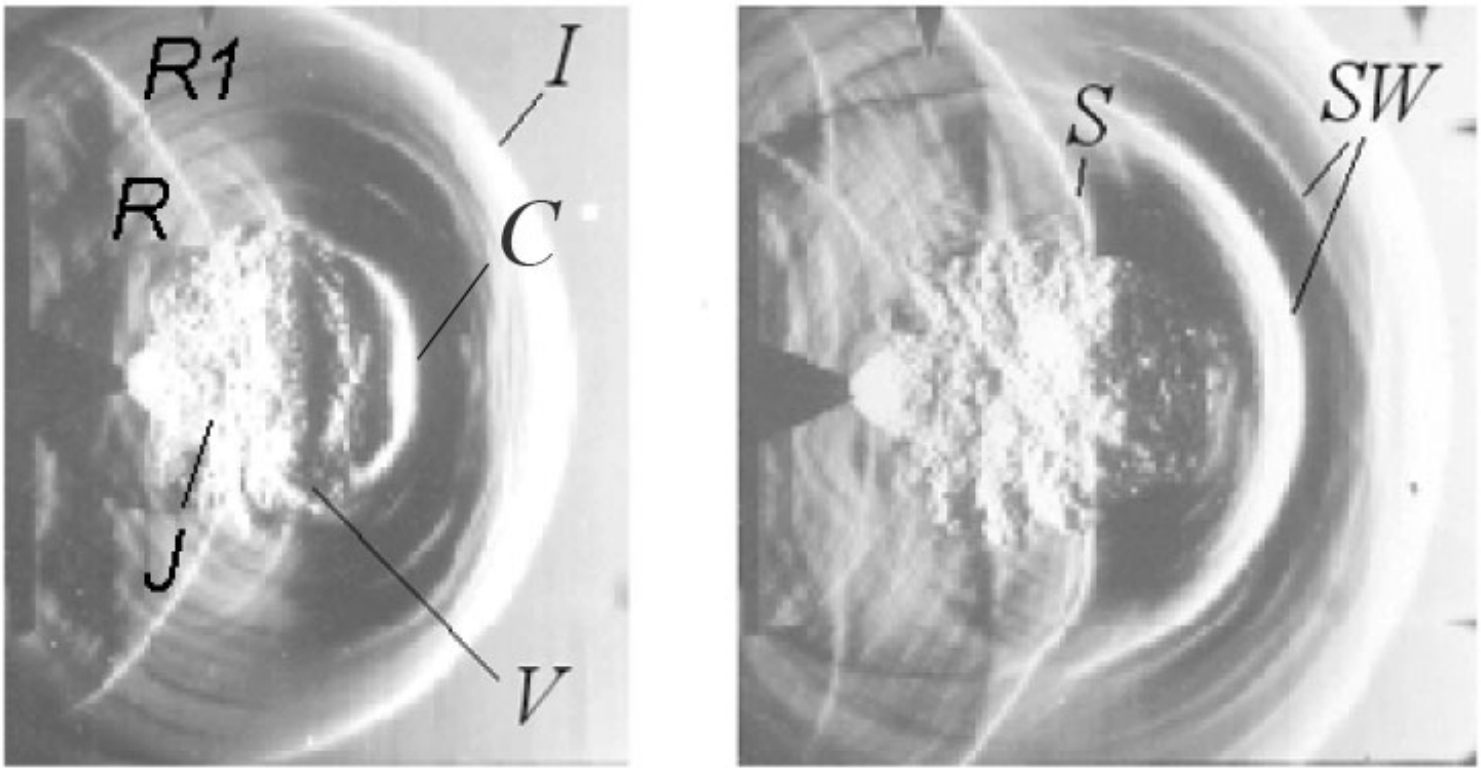

In front of the discharging gas the starting shock wave *I* is propagating, generating the movement of the ambient gas and heating it.

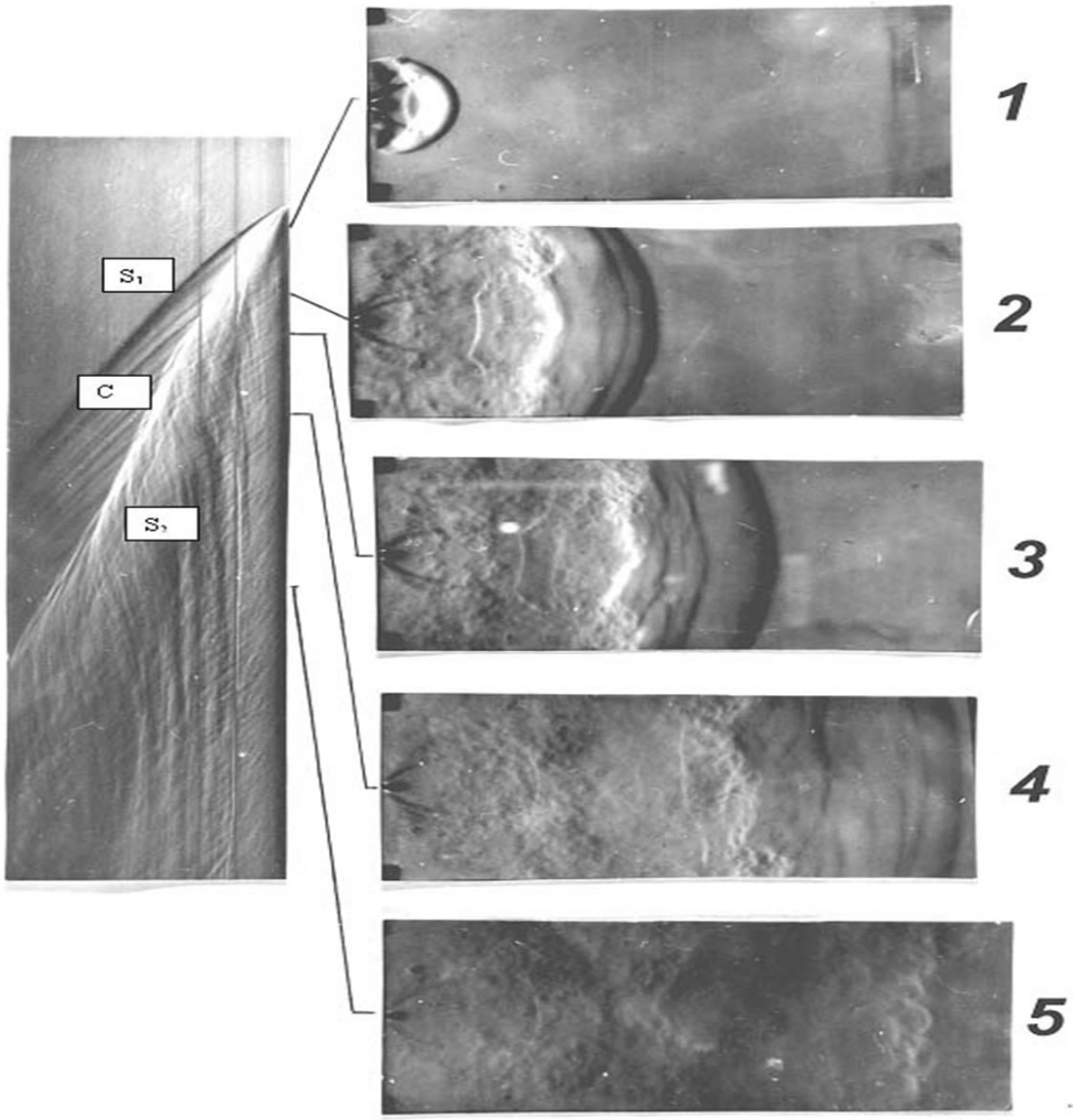

Streak record and schlieren photographs of impulse jet formation

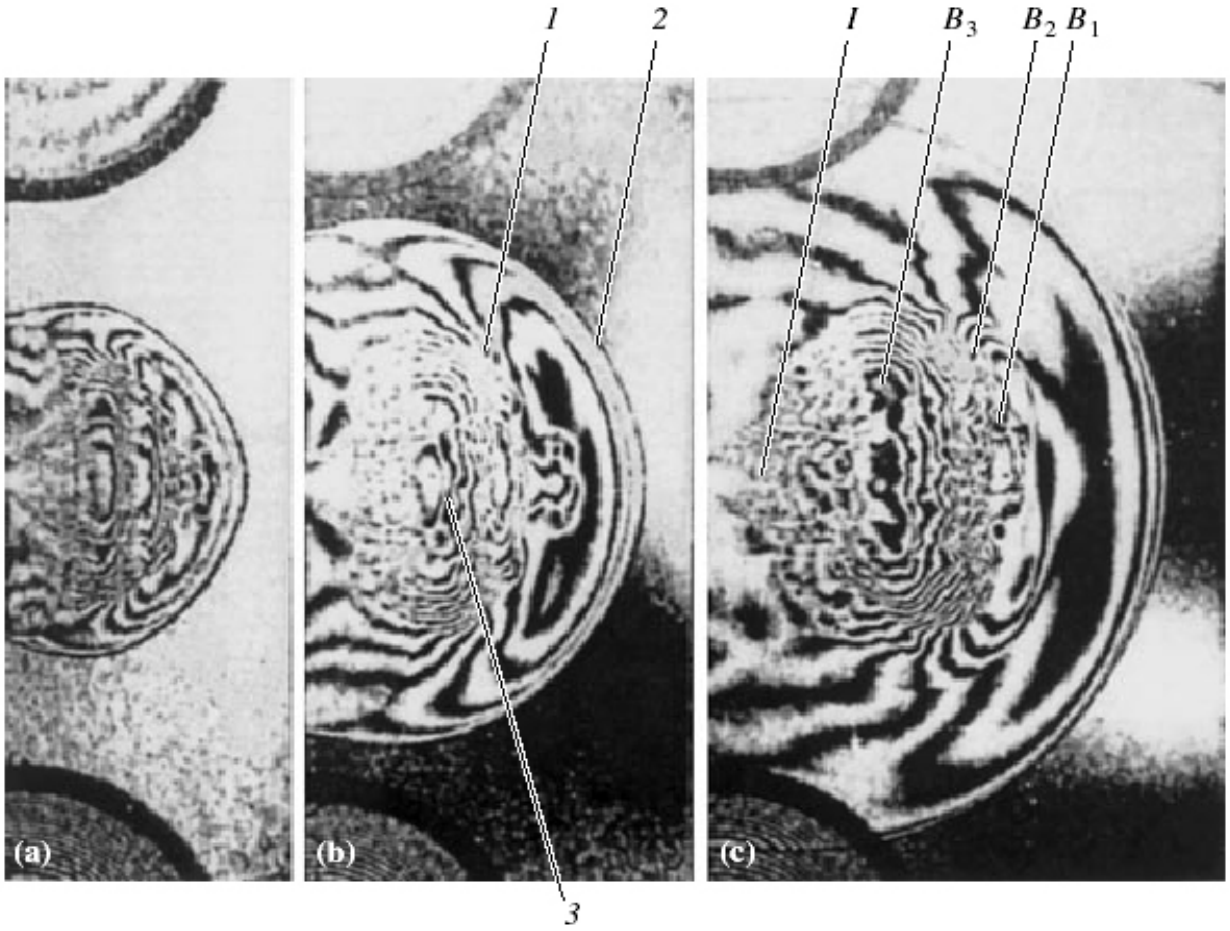

Interferogramms illustrating the development of a pulsed nitrogen jet emitted from a sonic nozzle with an input pressure of 34 bar into atmosphere: (*1*) contact surface; (*2*) starting shock wave; (*3*) secondary shock wave; (*I*) isentropic expansion core; (*B1, B2, B3*) vortex rings. Patterns (a), (b), and (c) refer to the moments of time 40, 64, and 98 μs after discharge start.

Sketch of the Impulse Jet Structure

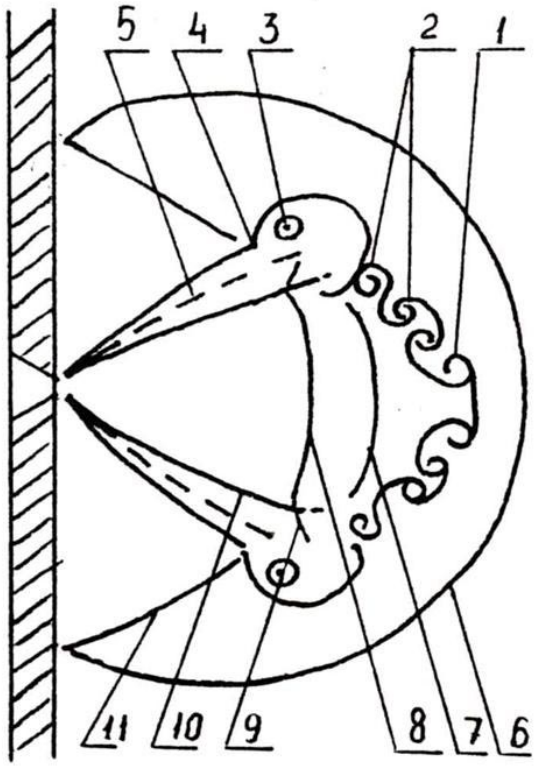

The contact surface 1 separates the gas heated by the shock wave from expanding gas from the nozzle.
The contact surface is strongly turbulent which favours mixing of expanding cold gas and hot gas behind the primary shock wave.

Numerical simulation an impulse jet

In order to detect regions of mixing of discharged cold hydrogen and hot air behind the starting shock wave the numerical simulation of non-steady-state flow of ideal gas was carried out.

$$\frac{\partial}{\partial t}\int_{\Omega}\rho d\Omega = \int_{G}\rho\vec{v}dG \qquad \frac{\partial}{\partial t}\int_{\Omega}\rho\vec{v}d\Omega = \int_{G}(\rho\vec{v}*\vec{v}+P)dG$$

$$\frac{\partial}{\partial t}\int_{\Omega}\rho E d\Omega = \int_{G}\rho\vec{v}(E+P/\rho)dG$$

The numerical modeling of flow investigated was carried out by means of Euler equations solution using second order of approximation Steger-Worming scheme. Two components dynamics and mixing were considered.

Density field in the impulse sonic jet

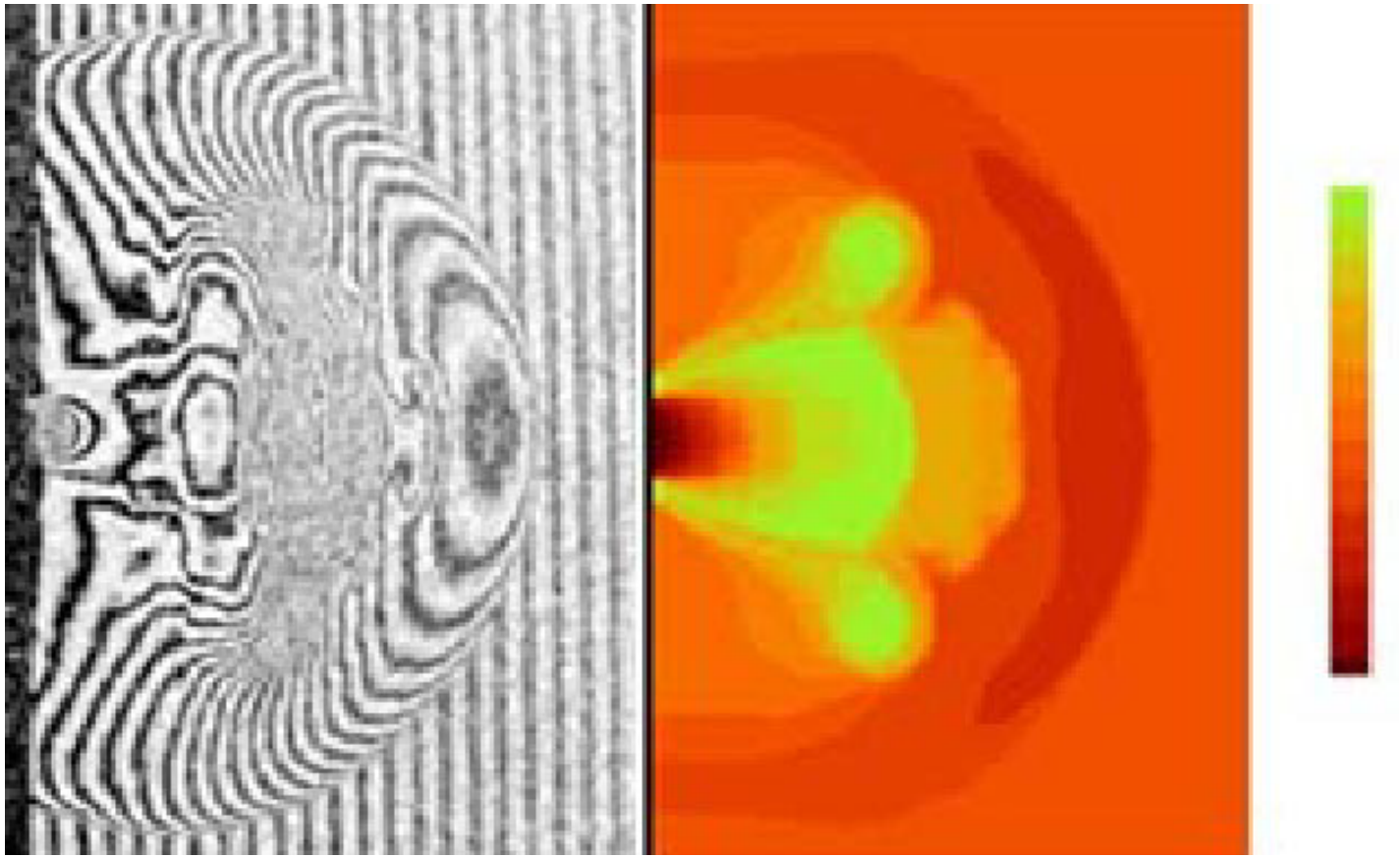

The numerical results (right) are compared with the experimental ones(left) (Ma=1, n=18, t = 50μs)

Density distribution in impulse jet

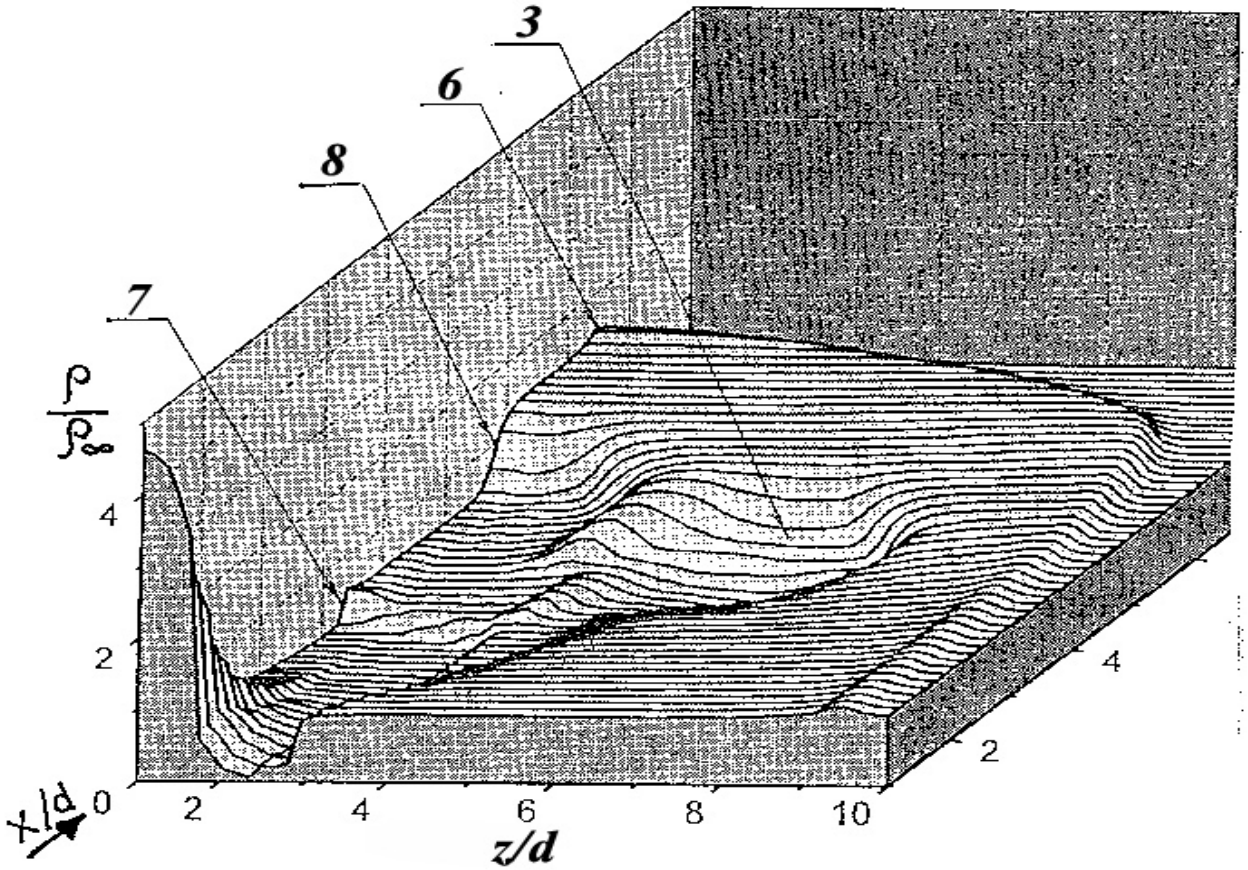

(Ma=1, n=18, t = 50μs)

Density of ambient gas – oxygen (top) and discharging gas – hydrogen (bottom) at the time of 1.5 non-dimensional units.

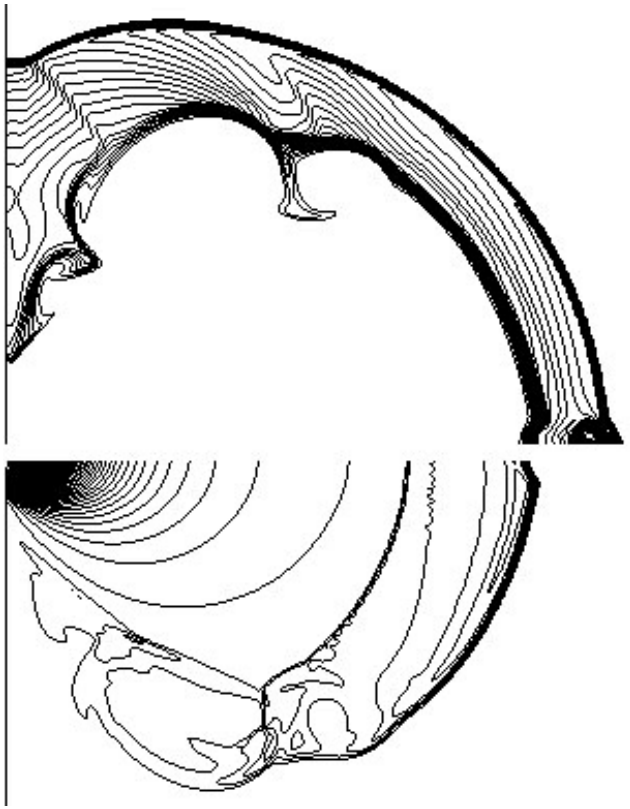

The initial conditions are: pressure ratio – 200,
temperature ratio – 1, specific heat ratios of both gases – 1.4

Temperature distribution at the time of 1.5 non-dimensional units

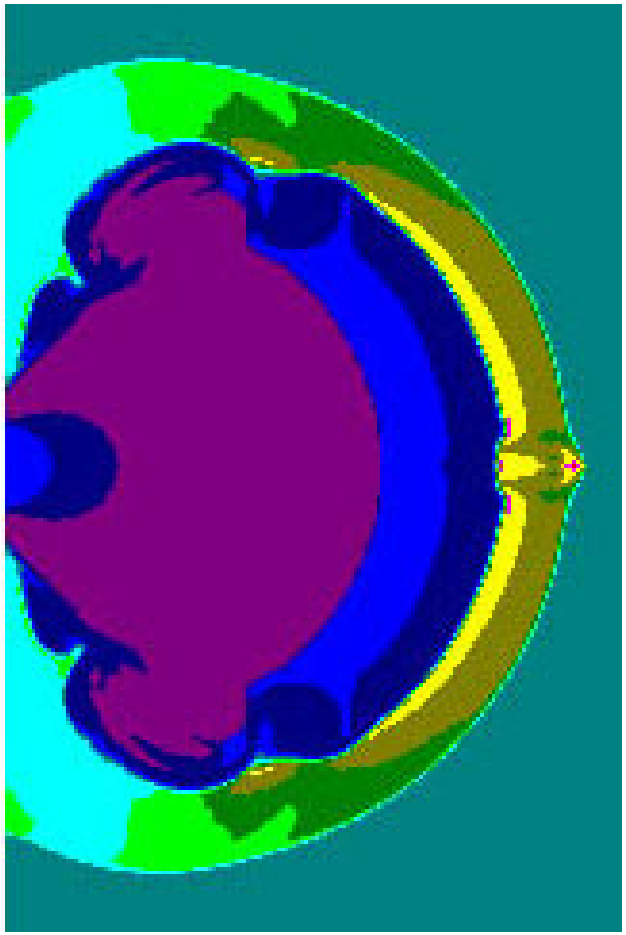

The initial conditions are: pressure ratio – 200,
temperature ratio – 1, specific heat ratios of both gases – 1.4

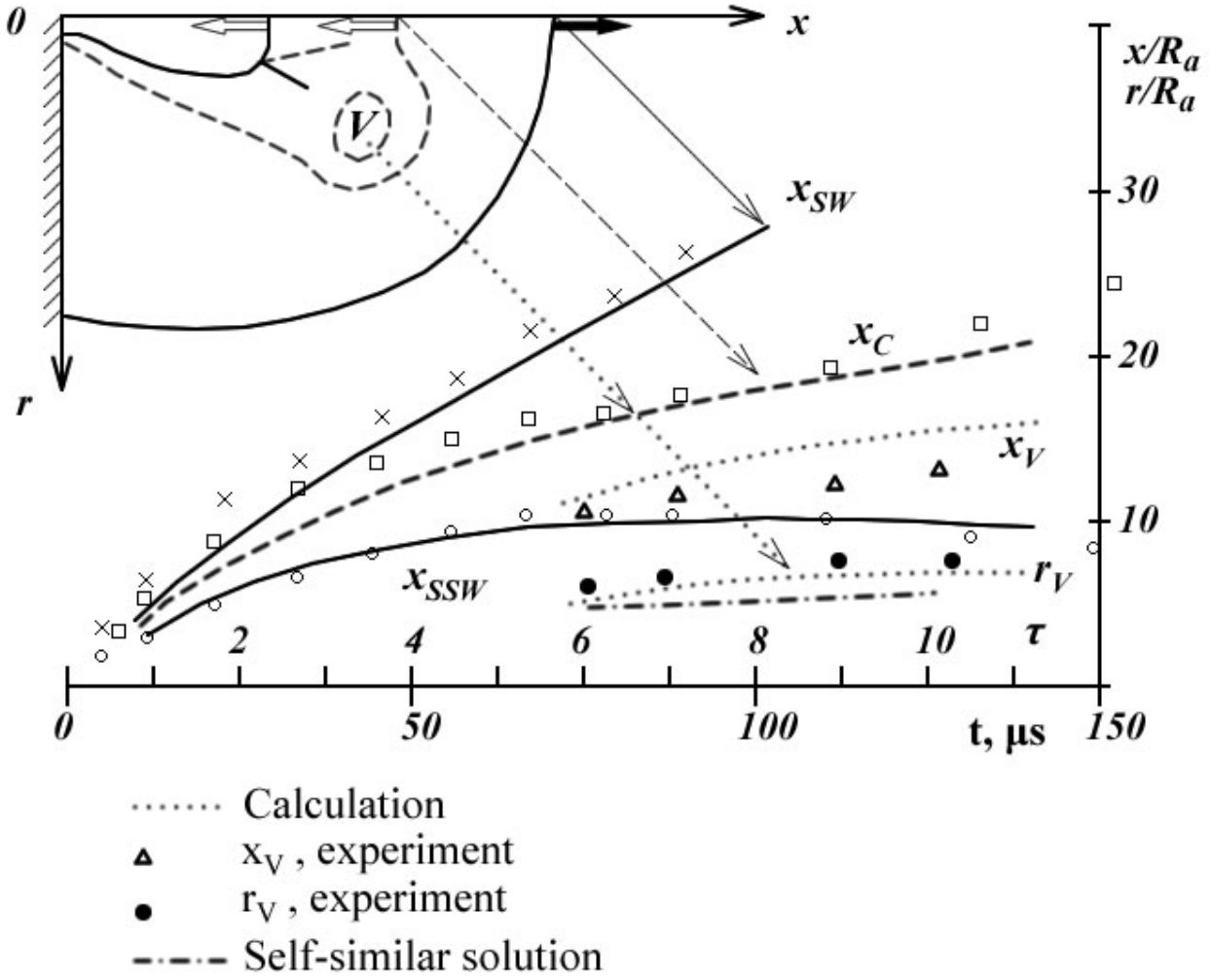

Experimental and calculated trajectory of starting shock wave, contact surface and secondary shock wave. (Ma=1, n=18).

Numerical simulation of hydrogen self-ignition

Calculations of the self-ignition of a hydrogen jet were based on a physicochemical model involving the gasdynamic transport of a viscous gas, the kinetics of hydrogen oxidation, the multicomponent diffusion, and heat exchange. The system of equations describing the chemical kinetics included nine equations. For the solution of combustion gasdynamics tasks the method was modified that provided carrying out of stable calculations of second-order accuracy with respect to spatial coordinates. The system of chemical kinetics equations was solved using the Gear's method. The developed algorithm was implemented using FORTRAN-90.

System of equations is given by:

$$\frac{\partial \rho}{\partial t}+\frac{\partial(\rho u_r)}{\partial r}+\frac{\partial(\rho u_z)}{\partial z}+\frac{\rho u_r}{r}=0$$

$$\frac{\partial c_i}{\partial t}+u_r\frac{\partial c_i}{\partial r}+u_z\frac{\partial c_i}{\partial z}=\frac{1}{\rho}\left[\frac{1}{r}\frac{\partial}{\partial r}\left(r\rho D_i\frac{\partial c_i}{\partial r}\right)+\frac{\partial}{\partial z}\left(\rho D_i\frac{\partial c_i}{\partial z}\right)\right]+\left(\frac{\partial c_i}{\partial t}\right)_{chem}$$

$$\rho\left(\frac{\partial u_r}{\partial t}+u_r\frac{\partial u_r}{\partial r}+u_z\frac{\partial u_r}{\partial z}\right)=-\frac{\partial p}{\partial r}+\frac{\partial \sigma_{rr}}{\partial r}+\frac{\partial \sigma_{rz}}{\partial z}+\frac{\sigma_{rr}-\sigma_{\varphi\varphi}}{r}$$

$$\rho\left(\frac{\partial u_z}{\partial t}+u_r\frac{\partial u_z}{\partial r}+u_z\frac{\partial u_z}{\partial z}\right)=-\frac{\partial p}{\partial z}+\frac{\partial \sigma_{rz}}{\partial r}+\frac{\partial \sigma_{zz}}{\partial z}+\frac{\sigma_{rz}}{r}$$

$$\rho\left(\frac{\partial E}{\partial t}+u_r\frac{\partial E}{\partial r}+u_z\frac{\partial E}{\partial z}\right)=-\left(\frac{1}{r}\frac{\partial}{\partial r}(rpu_r)+\frac{\partial(pu_z)}{\partial z}\right)+\frac{\partial}{\partial r}(\sigma_{rr}u_r+\sigma_{rz}u_z)+$$

$$+\frac{\partial}{\partial z}(\sigma_{zr}u_r+\sigma_{zz}u_z)+\frac{1}{r}(\sigma_{rr}u_r+\sigma_{rz}u_z)+\frac{1}{r}\frac{\partial}{\partial r}\left(r\kappa(T)\frac{\partial T}{\partial r}\right)+$$

$$+\frac{\partial}{\partial z}\left(\kappa(T)\frac{\partial T}{\partial z}\right)+\sum_k\frac{h_k}{m_k}\left(\frac{1}{r}\frac{\partial}{\partial r}\left(r\rho D_k(T)\frac{\partial c_k}{\partial r}\right)+\frac{\partial}{\partial z}\left(\rho D_k(T)\frac{\partial c_k}{\partial z}\right)\right)$$

Where viscous tension tensor components are given by:

$$\sigma_{rr} = 2\mu\frac{\partial u_r}{\partial r} - \frac{2}{3}\mu\left(\frac{\partial u_r}{\partial r} + \frac{\partial u_z}{\partial z} + \frac{u_r}{r}\right)$$

$$\sigma_{\varphi\varphi} = 2\mu\frac{u_r}{r} - \frac{2}{3}\mu\left(\frac{\partial u_r}{\partial r} + \frac{\partial u_z}{\partial z} + \frac{u_r}{r}\right)$$

$$\sigma_{zz} = 2\mu\frac{\partial u_z}{\partial z} - \frac{2}{3}\mu\left(\frac{\partial u_r}{\partial r} + \frac{\partial u_z}{\partial z} + \frac{u_r}{r}\right)$$

$$\sigma_{zr} = \sigma_{rz} = \mu\left(\frac{\partial u_z}{\partial r} + \frac{\partial u_r}{\partial z}\right)$$

$$\sigma_{r\varphi} = \sigma_{\varphi z} = 0$$

u_r, u_z – velocity components, ρ – gas mixture density,

$c_i = \frac{n_i m_i}{\rho}$ – mass concentration of i-th component
(m_i – molar mass, n_i –molar density)

Mixture specific energy and pressure were calculated by the correlations for multicomponent mixtures

$$E = \varepsilon + \frac{1}{2}\left(u_r^2 + u_z^2\right)$$

$$\varepsilon = c_v T + \sum_k \frac{h_k n_k}{\rho} = c_v T + \sum_k h_k c_k$$

$$p = \tilde{R} T n = \left(\sum_i \frac{\tilde{R}_i}{m_i} c_i\right) \rho T = \rho T \sum_i R_i c_i$$

E, ε - total and intrinsic specific energies correspondingly,

h_i – specific enthalpy of i-th component formation,

p – pressure,

$c_v = \sum_i c_{vi} c_i$ – mixture specific heat capacity.

Transfer coefficients were determined according to kinetic gas theory and empirical correlations (Warnatz, Maas & Dibble, 2001)

$$\mu = \frac{1}{2}\left[\sum_i \alpha_i \mu_i + \left(\sum_i \frac{\alpha_i}{\mu_i}\right)^{-1}\right],$$ where $\alpha_i = \frac{n_i}{n}$ – molar part of i-th component

$$\mu_i = \frac{5}{16}\frac{\sqrt{\pi \hat{m}_i kT}}{\pi \sigma_i^2 \tilde{\Omega}_i^{(2,2)}}$$ – viscosity coefficient of i-th component,

$\tilde{\Omega}^{(2,2)}$ – reduced collisions integral, depending on reduced temperature $T^* = kT/\varepsilon^*$

and calculated for Lenard-Johnes potential
(ε* - constant in Lenard-Johnes potential),

$\hat{m}_i$ – mass of i-th component molecule, σ_i – molecule size.

Warnatz J., Maas U., & Dibble R.W. (2001). *Combustion. Physical and Chemical Fundamentals, modelling and simulations, experiments, pollutant formation.* Berlin:Springer.

Heat conductivity coefficient is determined in a similar manner to μ

$$\kappa = \frac{1}{2}\left[\sum_i \alpha_i \kappa_i + \left(\sum_i \frac{\alpha_i}{\kappa_i}\right)^{-1}\right], \text{ where } \kappa_i = \frac{\mu_i c_{pi}}{Pr} - \text{ i-th component heat conductivity coefficient .}$$

i-th component diffusion coefficient in multicomponent mixture is defined as

$$D_i = \frac{1 - c_i}{\sum_{i \neq j} \alpha_i / D_{ij}}, \text{ where}$$

$$D_{ij} = \frac{3}{8} \frac{\sqrt{2\pi k T \hat{m}_i \hat{m}_j / (\hat{m}_i + \hat{m}_j)}}{\pi \sigma_{ij}^2 \tilde{\Omega}^{(1,1)}(T_{ij}^*)} \cdot \frac{1}{\rho} \quad - \text{ binary diffusion coefficient.}$$

In this equation

$$T_{ij}^* = \frac{kT}{\varepsilon_{ij}^*} \qquad \sigma_{ij} = 0{,}5(\sigma_i + \sigma_j) \qquad \varepsilon_{ij}^* = \sqrt{\varepsilon_i^* \varepsilon_j^*}$$

$\tilde{\Omega}_{ij}^{(1,1)}$ – analogue of collision integral $\tilde{\Omega}^{(2,2)}$

$\left(\frac{dc_m}{dt}\right)_{chem}$ – variation of m-th chemical component part at the expense of chemical reactions described by the kinetic equations system in general form

$$\frac{dc_m}{dt} = F_m(c_1,...,c_M,T), \quad m = 1,...,M, \qquad F_m = \sum_{k=1}^{K}(\beta_{mk} - \alpha_{mk})w_k(c,T)$$

$$w_k = k_{fk}(T)\prod_{i=1}^{M} c_i^{\alpha_{ik}} - k_{bk}(T)\prod_{j=1}^{M} c_j^{\beta_{jk}}$$

according the chosen scheme of chemical reactions.

$$\sum_{i=1}^{M}\alpha_{ik}A_i = \sum_{j=1}^{M}\beta_{jk}B_j \qquad k=1,...,K,$$

where K – number of equations describing chemical reactions,

α_{ik} и β_{jk} – stoichiometric coefficients of k–th reaction.

Speeds of direct and reverse reactions $k_{fk}(T)$ и $k_{bk}(T)$ are correlated with the detailed equivalence principle and given by $k(T) = AT^N \exp(-\frac{E_{act}}{RT})$

Initial conditions

Simulation of mixing and combustion of hydrogen jet, discharging from the reservoir at initial temperature T = 300 K, pressure P = 150-400 bar, hole diameter d = 1-4 mm and hot air behind the starting shock wave was considered. Computational grids with a cell size of 0.04-0.1 mm

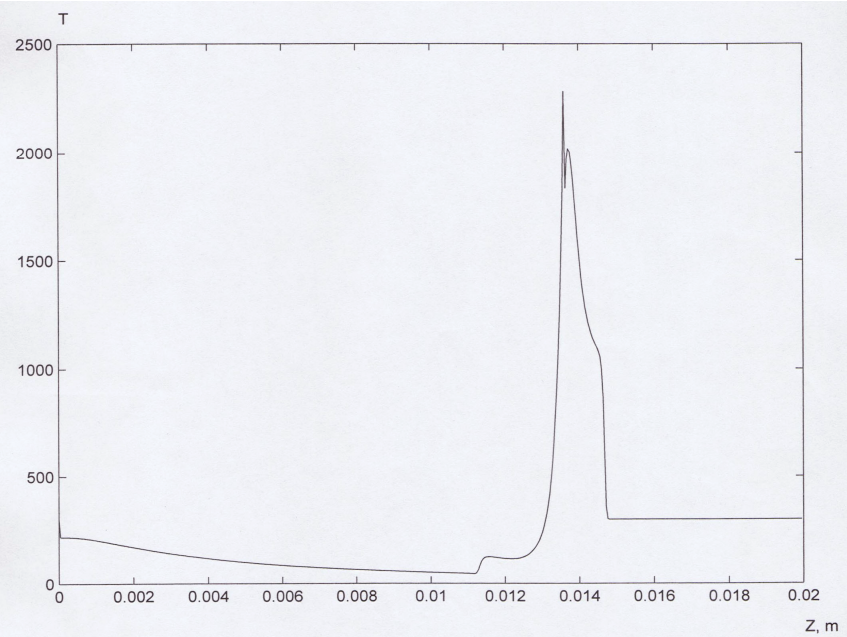

Temperature distribution along the jet

The temperature in the hot zone increases due to generation of heat in the chemical reactions up to 2400 K

Calculated H_2O concentration distribution related to the H_2O concentration in fully combusted mixture

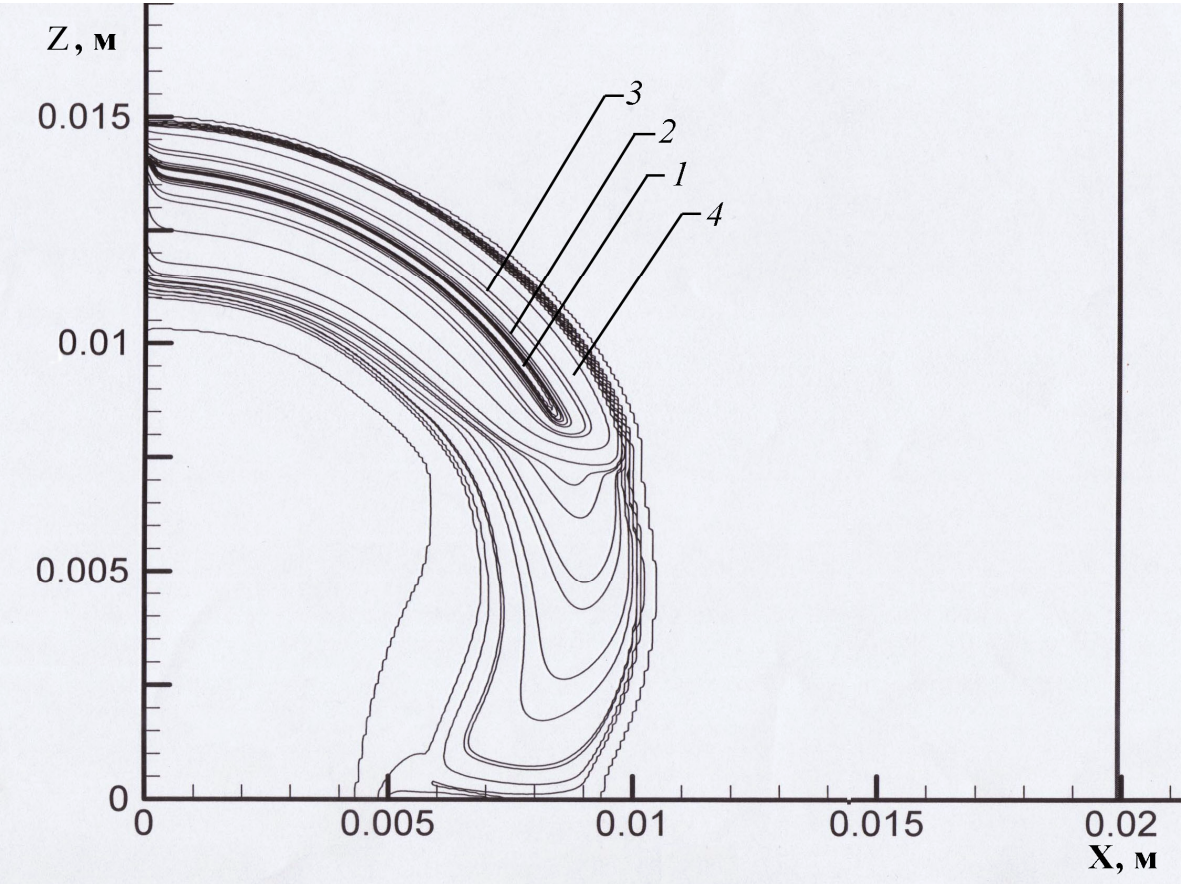

Z , X – distance from the orifice along and normal to the flow direction. Isolines 1-4 correspond to 70, 30, 10, and 2% respectively. t = 8 μs

Concentrations of species along the jet

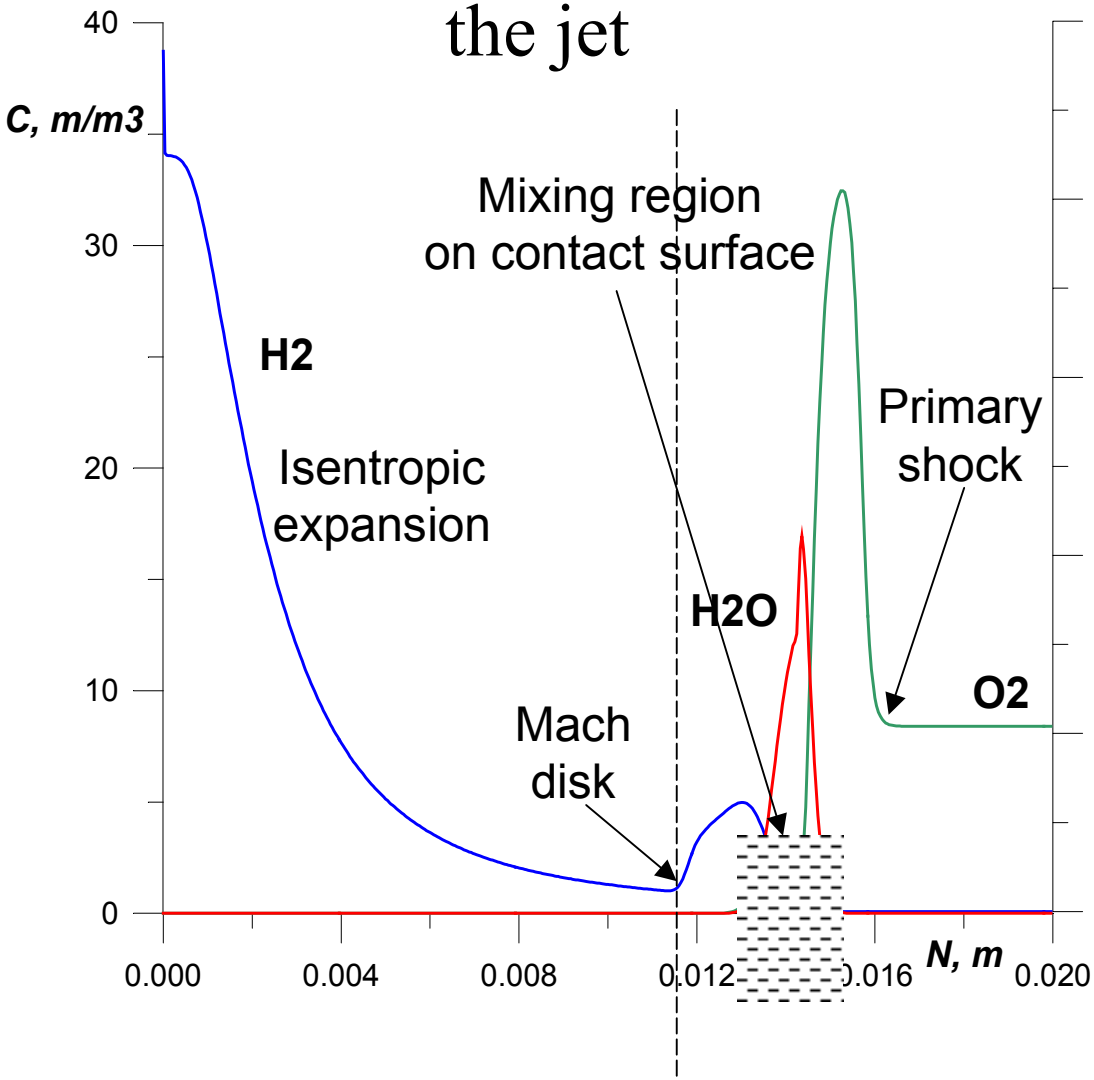

P_0 = 400 atm
d = 4 mm
t = 8μs

Maximum temperature-time distributions

Discharging and ambient gas temperatures 300 K,

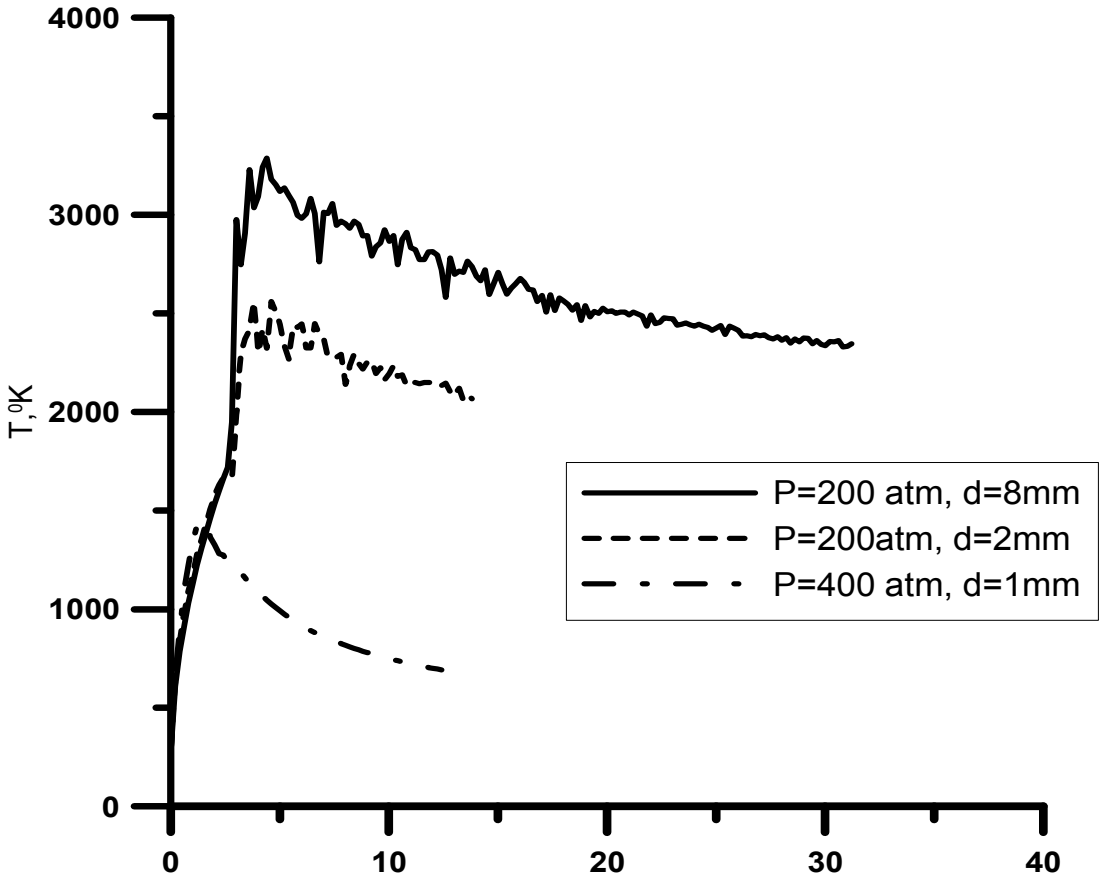

– ignition occurs followed by steady-state

– ignition occurs, but extinction is expected

– no ignition and no combustion (reservoir pressure

Conclusions

- The possible reason of combustible gas self-ignition could be the gas ignition on the contact surface separating discharging gas from surrounding oxidizer heater by the primary shock wave.
- The self-ignition in the emitted jet takes place if the initial hydrogen pressure in the vessel on the order of 150-400 bar, temperature of hydrogen and surrounding gas (air) 300 K and the hole diameter is more than 3 mm. If, under the same initial temperature and pressure the hole diameter is 2.6 mm or less combustion breaks.
- The character of the observed process strongly depends on the initial temperature of hydrogen and air: the emitted jet exhibits self-ignition at an initial pressure of 200 bar and hole diameter 2 mm if the initial temperature of the environment is increased to 400 K.

Unsolved problem

Methods of the blast waves attenuation during technical opening of high pressure tank

Hydrogen self-ignition in tubes

Explosive questions:

- Is it possible the hydrogen self-ignition in tubes?
- Where and when will hydrogen self-ignition occur?
- Is there an influence of cross-section shape of tube on self-ignition?

Experimental investigation of self-ignition in tubes

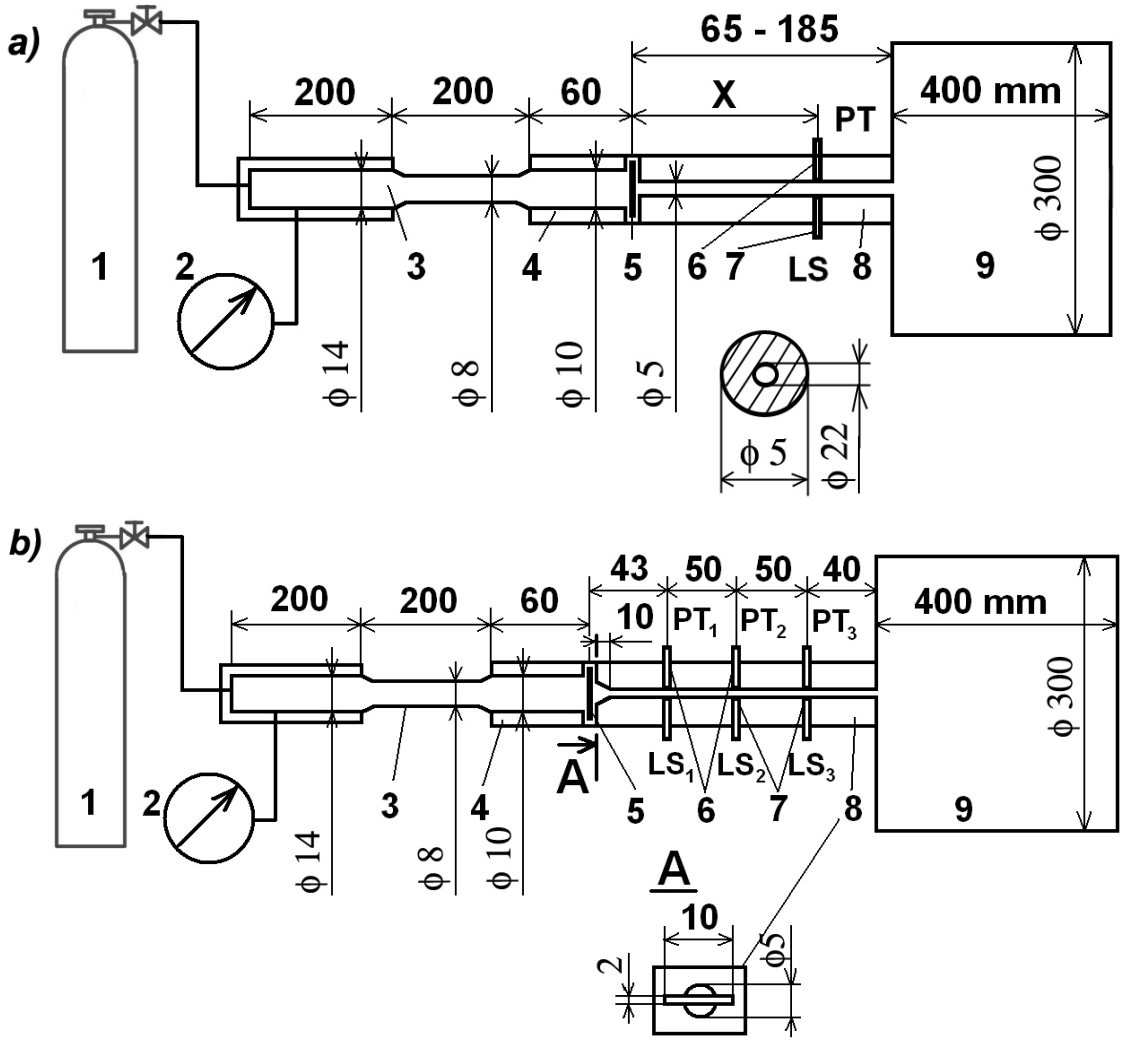

Schematic of experimental setups. a) low pressure tube of round cross section; b) low pressure tube of rectangular cross section. 1 – hydrogen bottle, 2 – manometer, 3 – high pressure chamber, 4 – diaphragm block, 5 – copper diaphragm (burst disk), 6 – pressure transducers (PT), 7 – light sensors (LS), 8 – low pressure chamber; 9 – buster chamber. X – distance between diaphragm and pressure transducer.

Low-pressure chamber of cylindrical cross-section

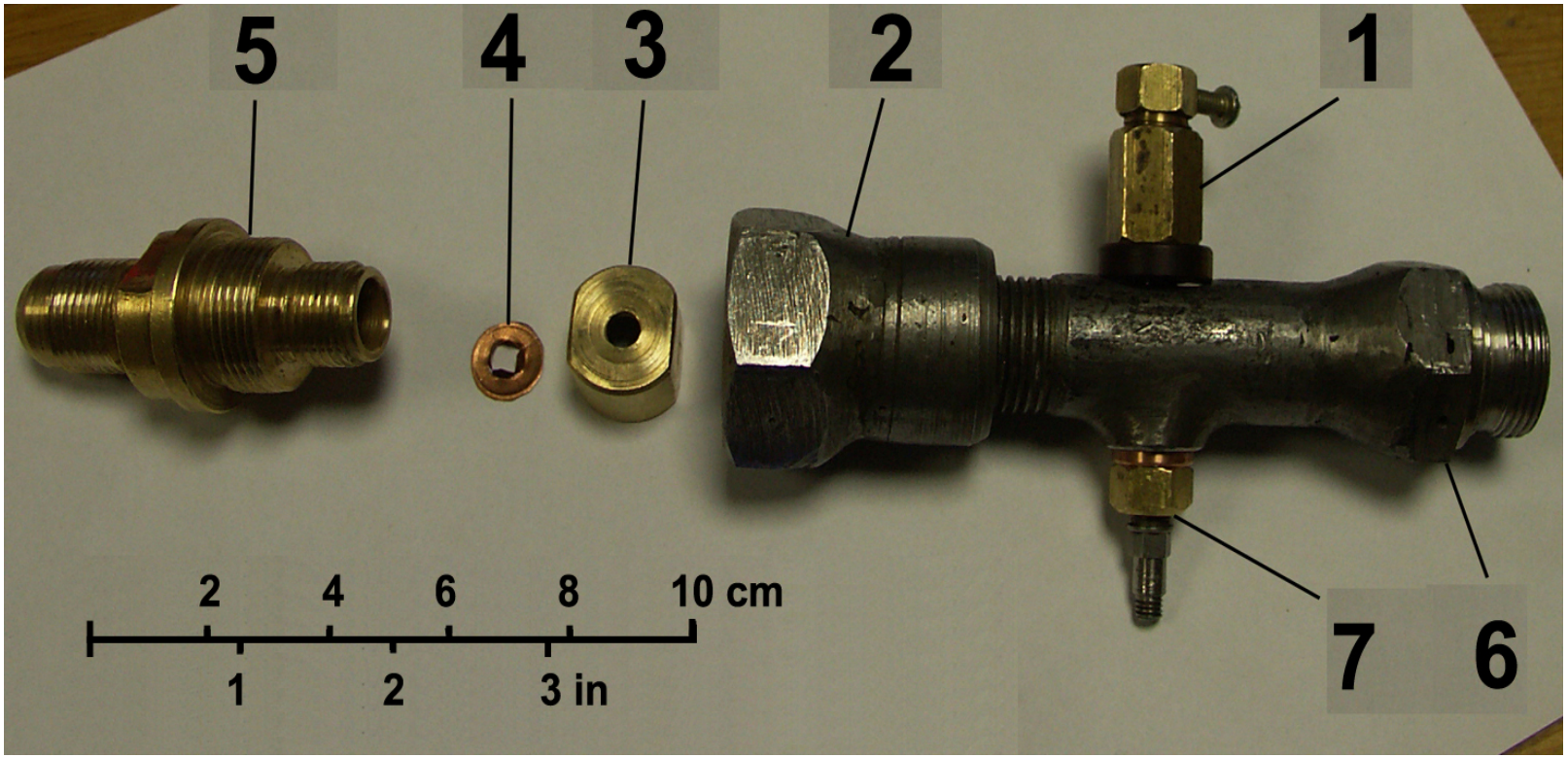

Picture of low-pressure chamber of round cross section. 1 – holder for light sensor, 2 – connector of the low-pressure tube with the diaphragm block, 3 – lock-nut with hole diameter of 5 mm, 4 – copper diaphragm of 10 mm in diameter, 5 – diaphragm block, 6 – the low-pressure chamber with connector to buster chamber, 7 – pressure transducer in holder.

Low-pressure chamber of rectangular cross-section

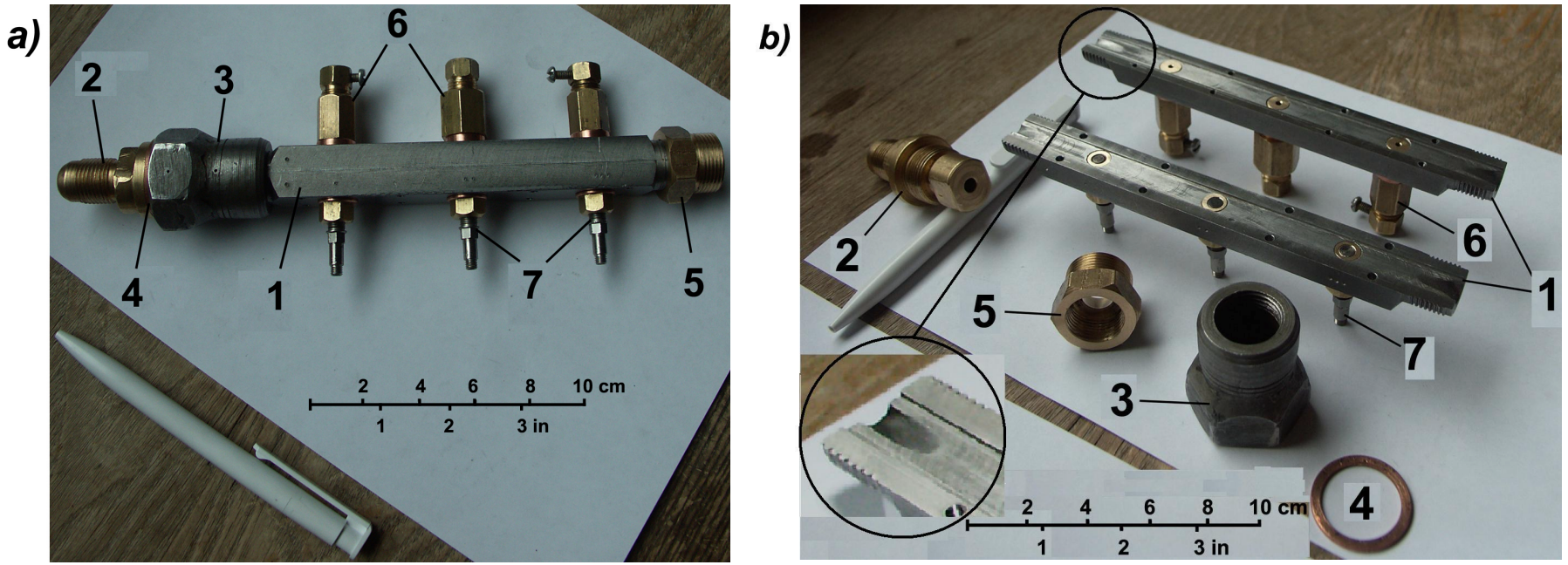

Picture of the low-pressure chamber of rectangular cross section (a) and its segments (b). 1 – segments of the low-pressure chamber, 2 – diaphragm block, 3 – connector of the low-pressure tube with the diaphragm block, 4 – copper gasket, 5 – connector of the low-pressure tube with the buster chamber, 6 – holders of light sensor, 7 – pressure transducers in holders.

Schematic of classical single pulse shock tube operation. (From Shapiro, 1954.)

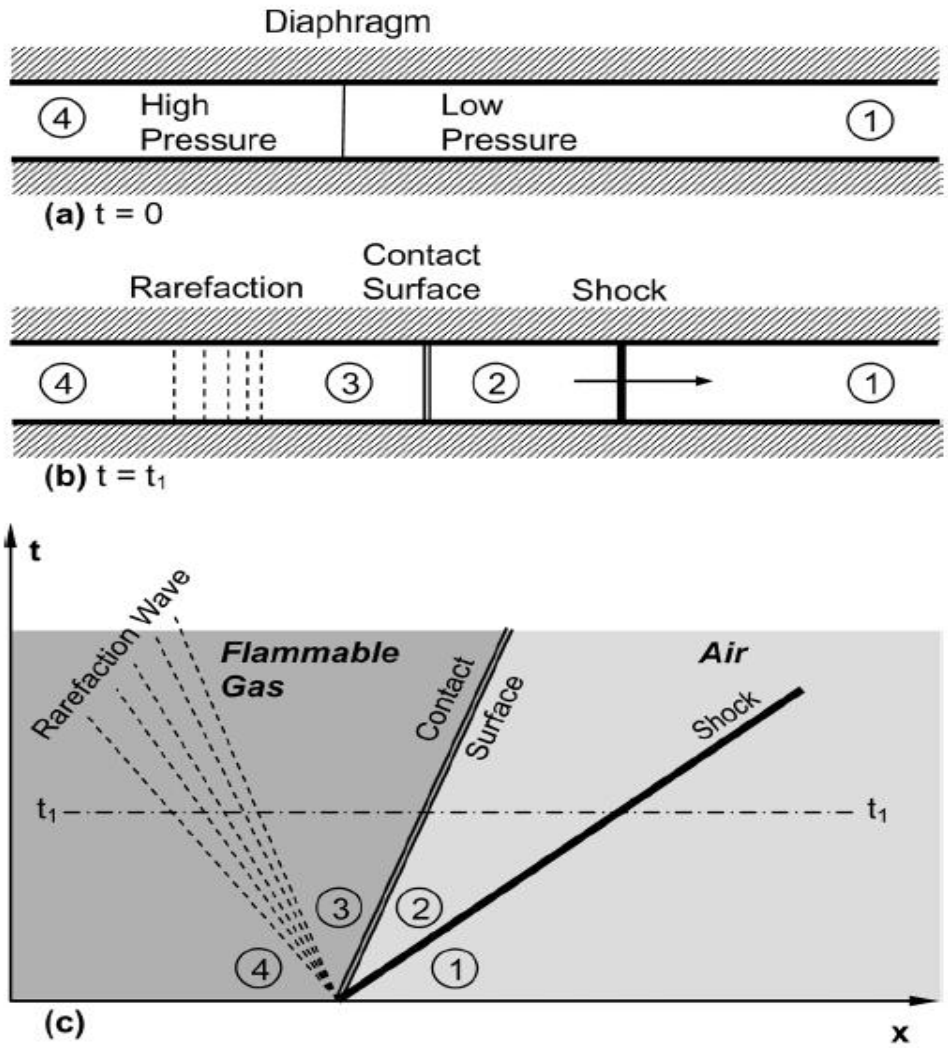

$$\upsilon_1 \equiv 0$$

$$u_1 = Ws$$

$$M_1 = \frac{u_1}{a_1} = u_1\left(\frac{\rho_1}{\gamma P_1}\right)^{1/2}$$

$$\frac{P_2}{P_1} = 1 + \gamma M_1^2\left(1 - \frac{\rho_1}{\rho_2}\right) \sim M_1^2$$

$$\frac{\rho_2}{\rho_1} = \frac{(\gamma+1)M_1^2}{(\gamma-1)M_1^2+2} \rightarrow \frac{\gamma+1}{\gamma-1} \approx 6(air)$$

$$\frac{T_2}{T_1} = \frac{P_2}{P_1}\cdot\frac{\rho_1}{\rho_2}$$

General equations of gas dynamics

$$\rho_1 u_1 = \rho_2 u_2$$

$$P_1 + \rho_1 u_1 = P_2 + \rho_2 u_2$$

$$H_1 + \frac{1}{2}u_1^2 = H_2 + \frac{1}{2}u_2^2$$

$$H = E + RT$$

$$H = \left(\frac{\gamma}{\gamma - 1}\right)RT = \left(\frac{\gamma}{\gamma - 1}\right)\frac{P}{\rho}$$

$$\frac{P_2}{P_1} = \frac{1 - \left(\frac{\gamma - 1}{\gamma + 1}\right)\frac{\rho_1}{\rho_2}}{\frac{\rho_1}{\rho_2} - \frac{\gamma - 1}{\gamma + 1}} = 1 + \frac{\rho_1 u_1^2}{P_1}\left(1 - \frac{\rho_2}{\rho_1}\right)$$

$$\frac{\rho_2}{\rho_1} = \frac{\frac{\gamma - 1}{\gamma + 1} + \frac{P_2}{P_1}}{\left(\frac{\gamma - 1}{\gamma + 1}\right)\frac{P_2}{P_1} + 1}$$

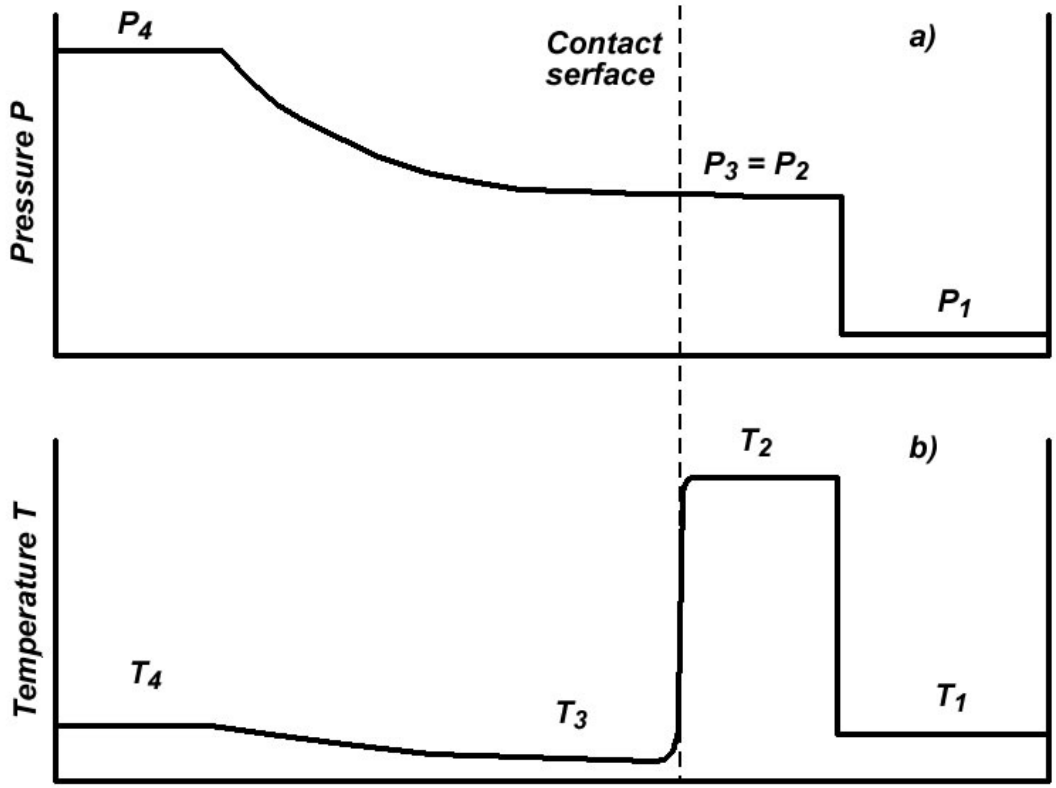

Pressure (a) and temperature (b) distribution along the tube at moment of time t1.

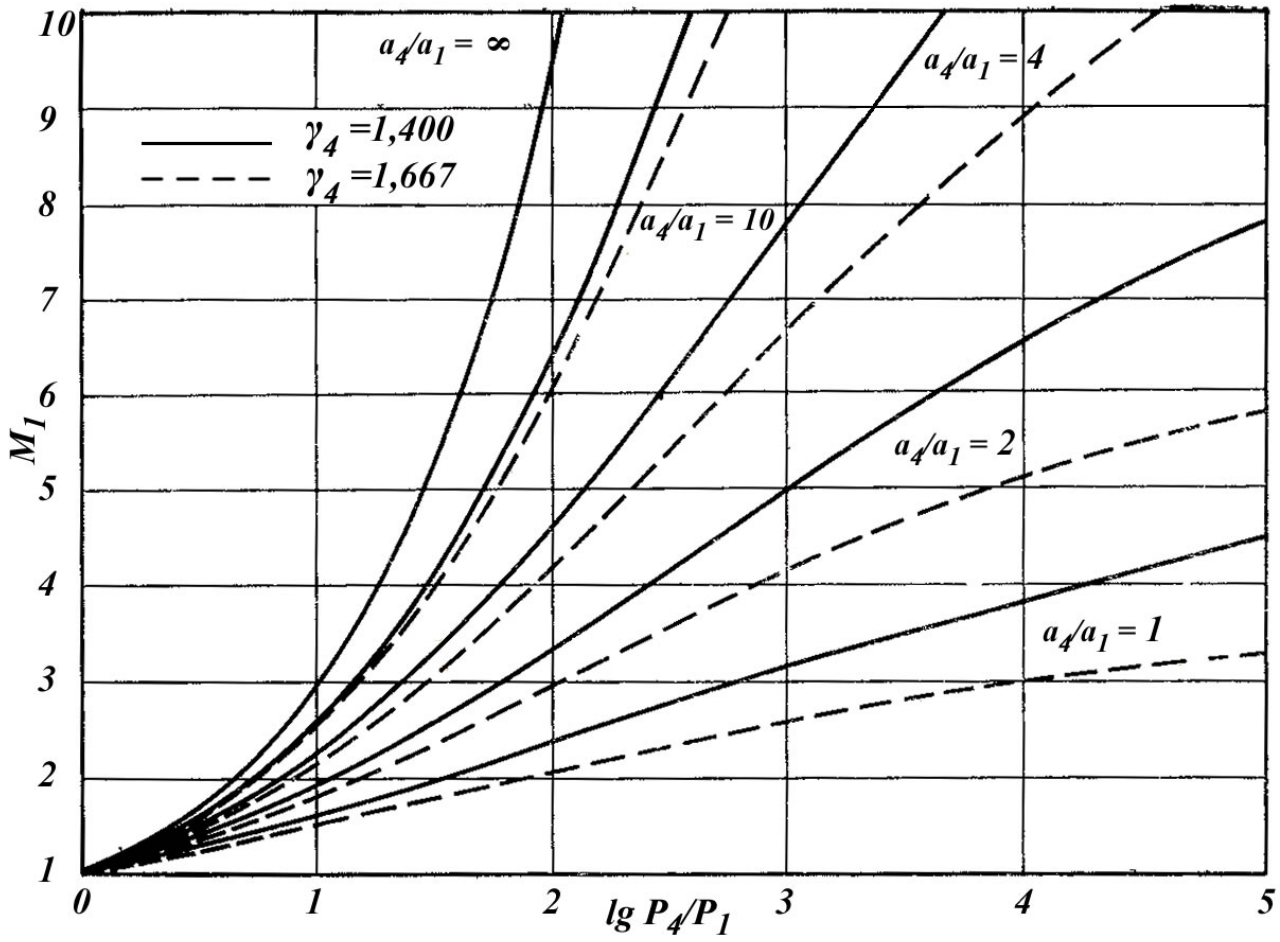

$$\frac{P_4}{P_1} = \frac{2\gamma_1 M_1^2 - (\gamma_1 - 1)}{\gamma_1 + 1}\left\{1 - \frac{\gamma_4 - 1}{\gamma_1 + 1}\frac{a_1}{a_4}\left(M_1 - \frac{1}{M_1}\right)\right\}^{-\frac{2\gamma_4}{\gamma_4 - 1}}$$

Self-ignition processes in rectangular tube

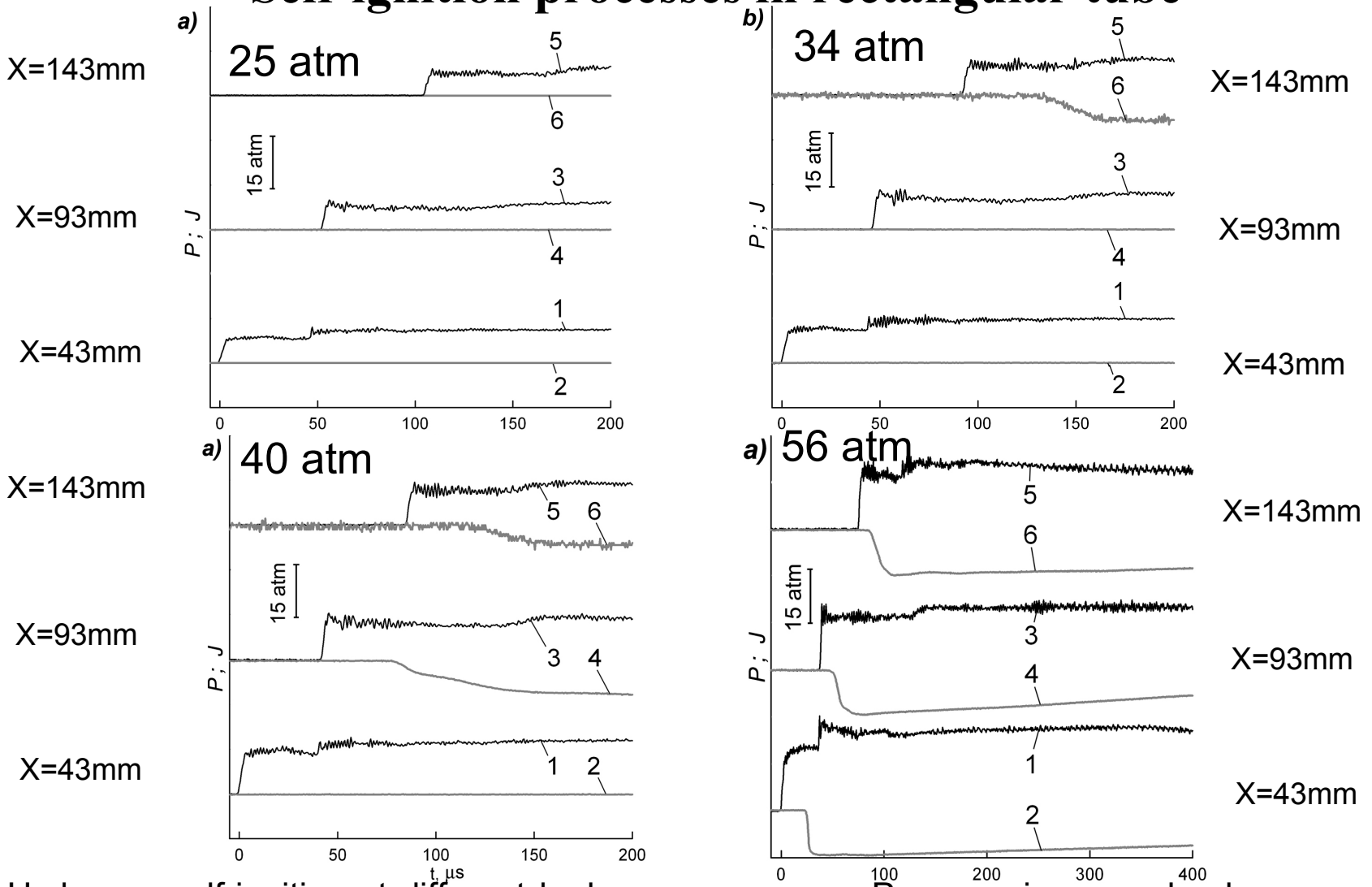

Hydrogen self-ignition at different hydrogen pressures. Pressure increase leads more close to the burst disk onset of combustion.

Self-ignition length in cylindrical tubes, role of hydrogen pressure

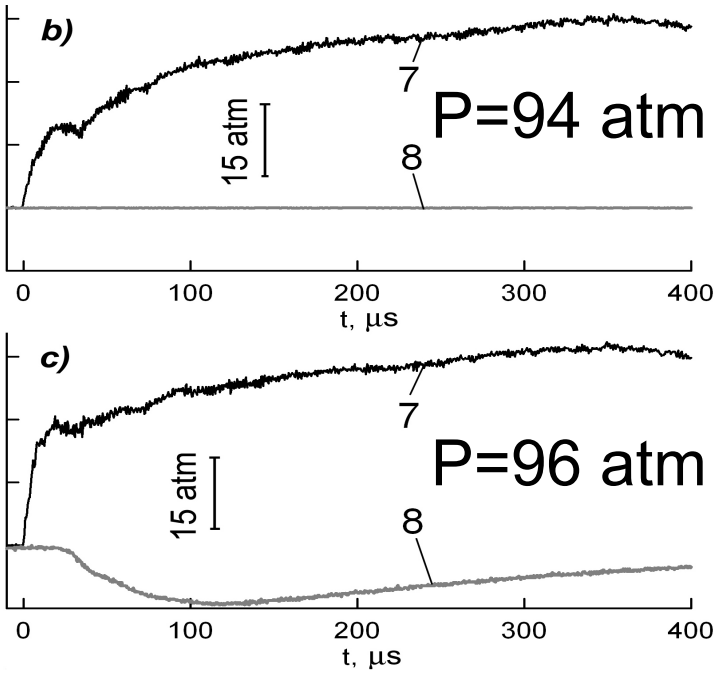

X=33 mm

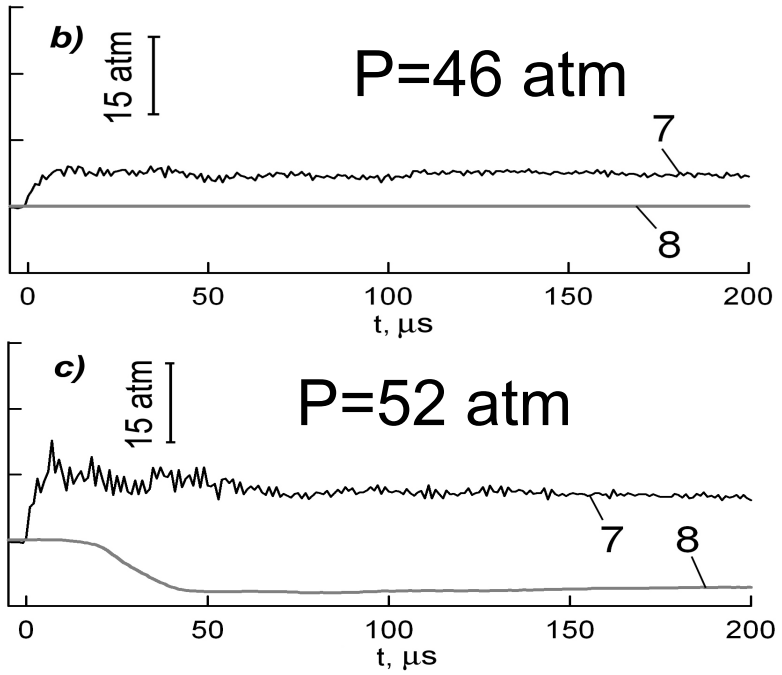

X=90 mm

7 – pressure signal,
8 – light signal.

Numerical simulation self-ignition of the hydrogen discharge into tube

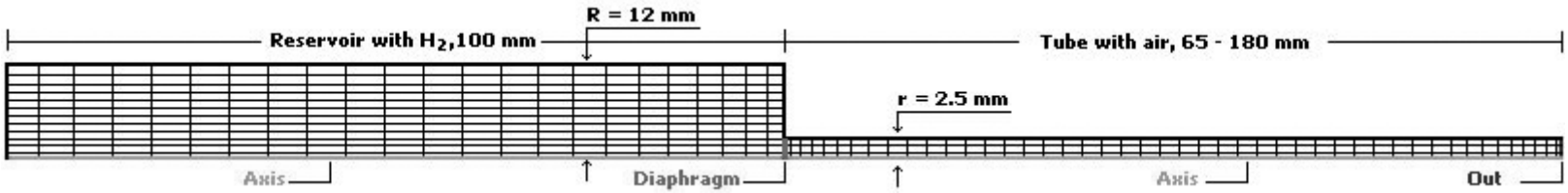

Calculation domain and grid example.

Grid influence

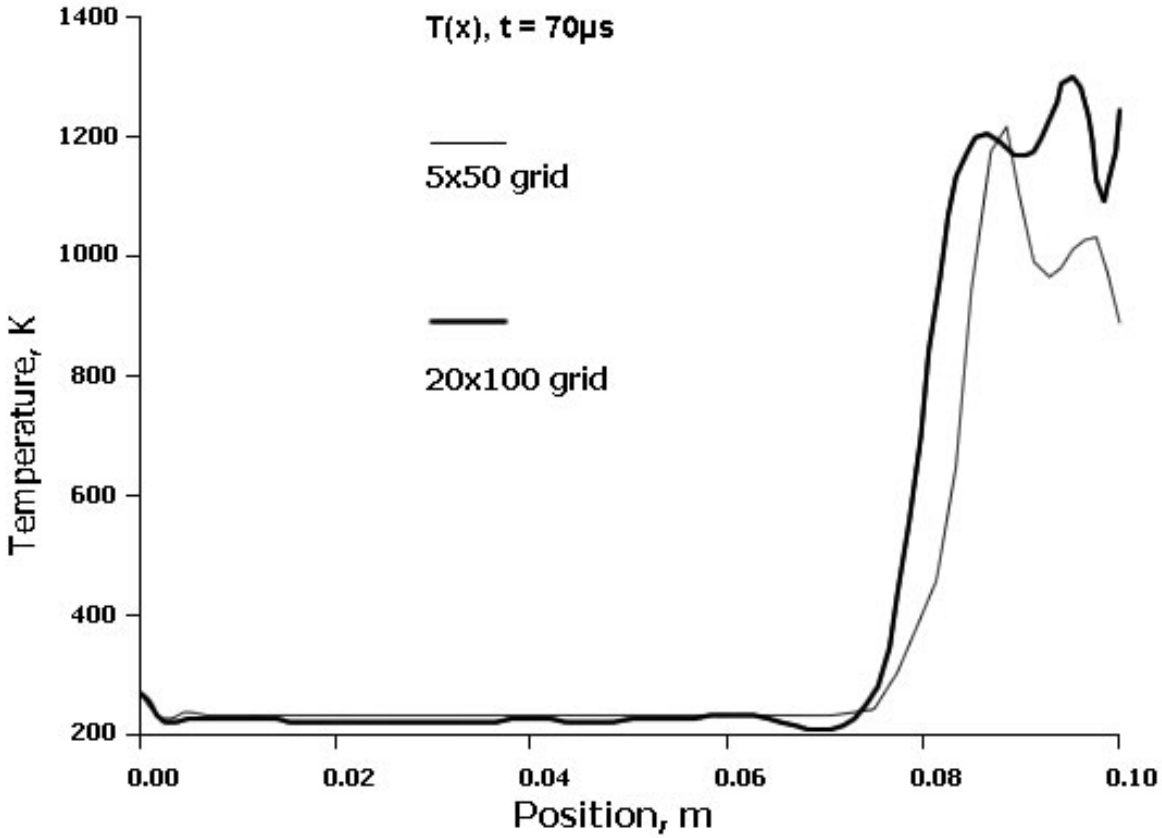

Calculated distributions of temperature along the tube for two calculation grids at time moment of 70 μs.

It is possible to make a conclusion about the acceptability of calculation with typical grids. For the numerical results obtained the convergence on the grids was checked, numerical viscosity effects were negligible.

Self-ignition evolution

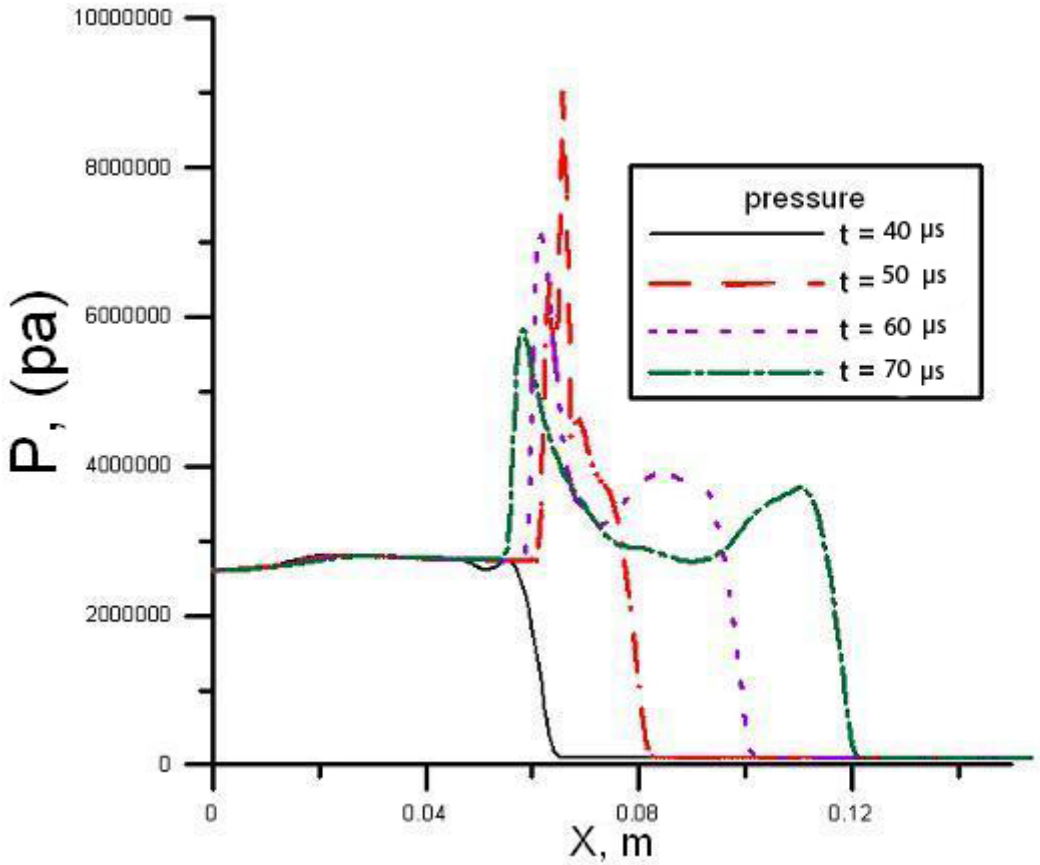

Calculated distributions of the pressure on the tube wall at different time moments.

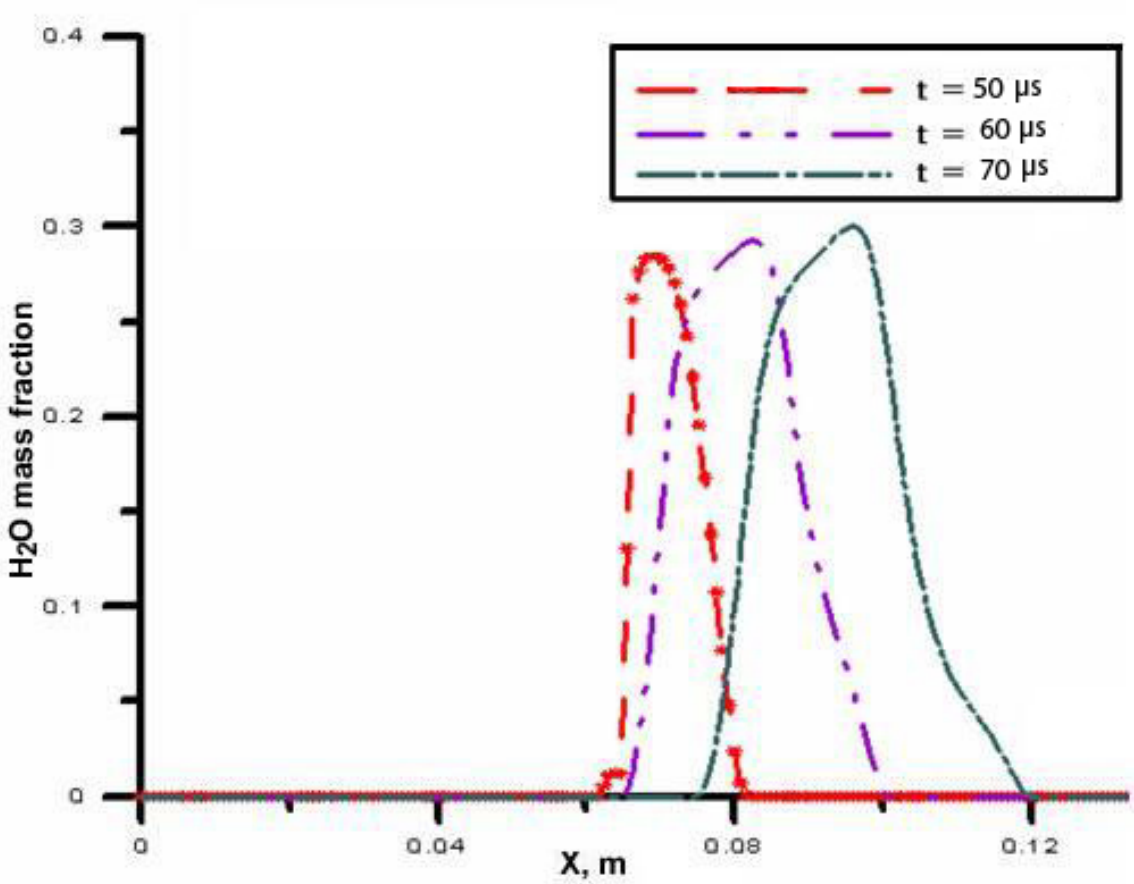

Calculated distributions of mass fraction of water vapour on the tube wall at different time moments.

Before the time moment of 40 μs the water concentration is about zero. After 50 μs the ignition with the subsequent combustion occurs. The water concentration increases to the value of about 0.3.

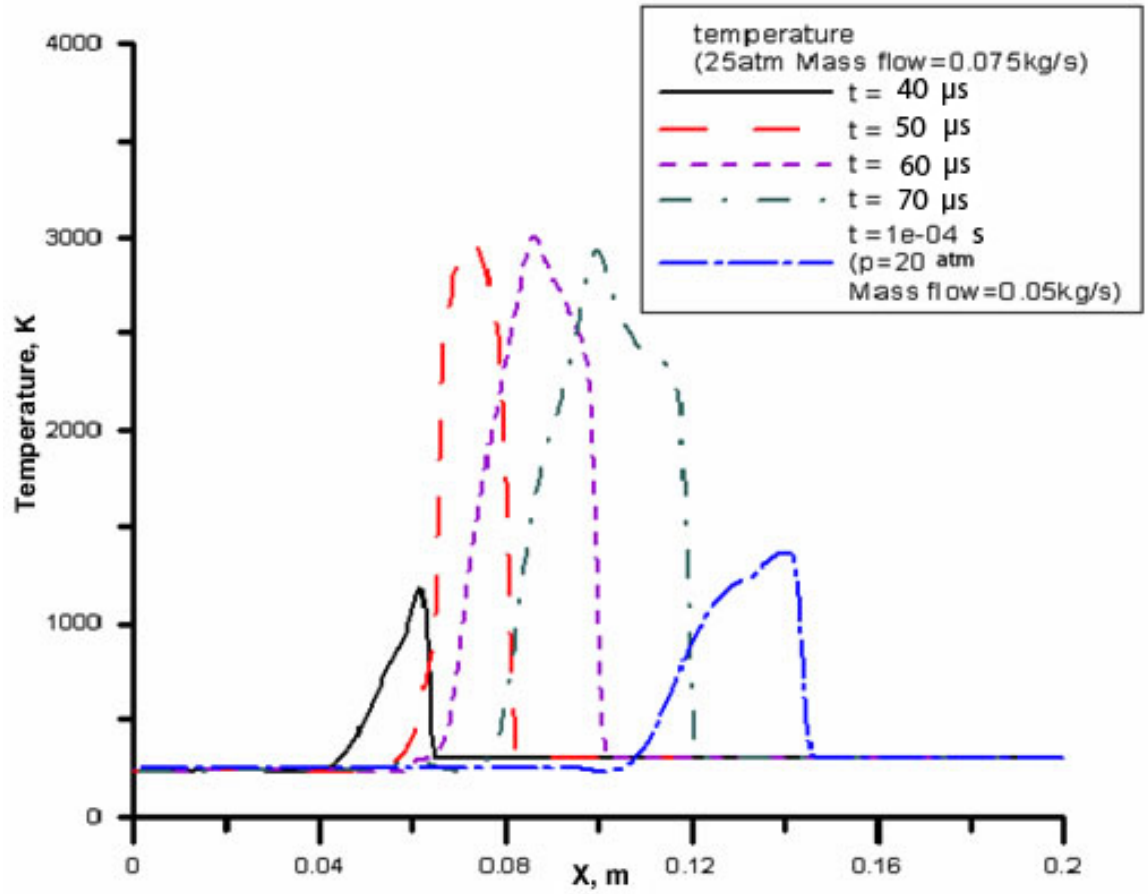

Calculated distributions of temperature on the tube wall at different time moments for two pairs of initial conditions (pressure – mass flow).

At the initial hydrogen pressure 50 atm case after 50 μs the ignition with the subsequent combustion occurs with the temperature increasing from 1200K to 3000K. But for the case (dashed blue curve) with initial pressure of 40 atm combustion is not occures.

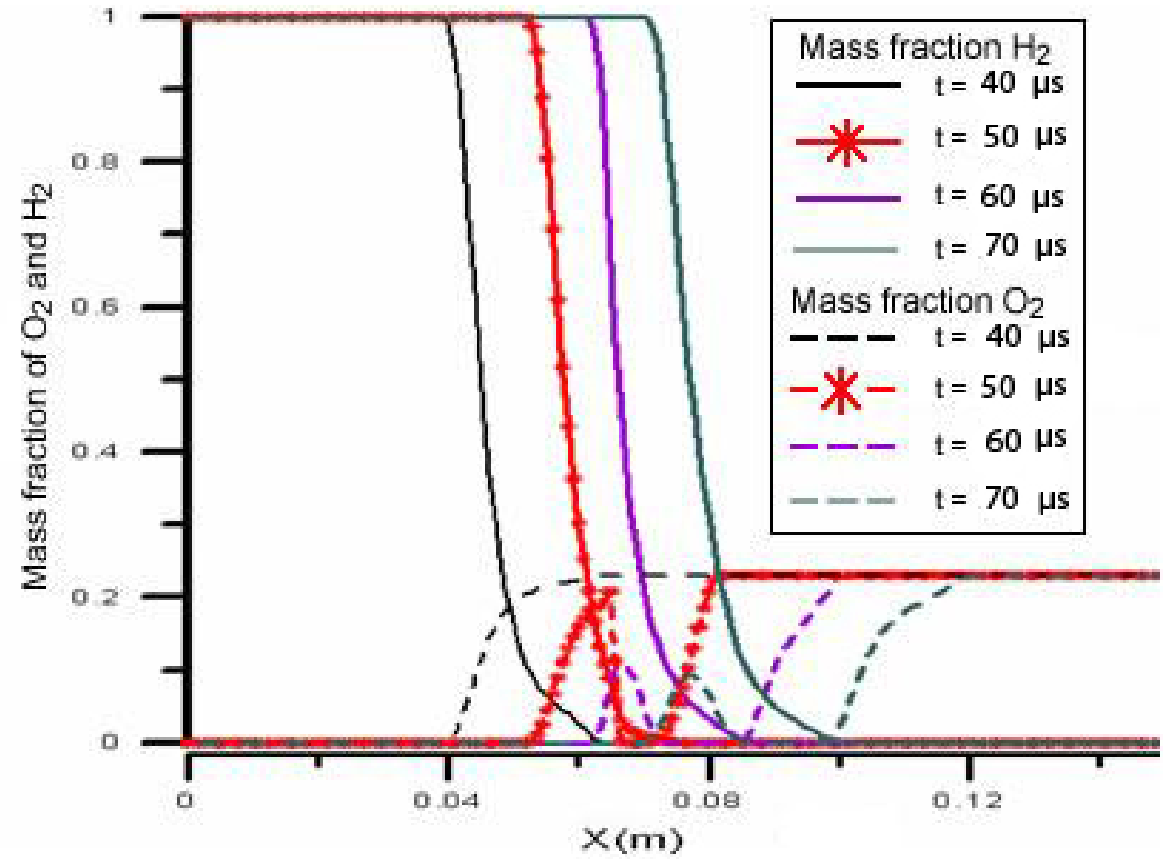

Calculated distributions of mass fraction of H_2 and O_2 on the tube wall at different time moments.

Figure demonstrates the process of ignition and subsequent combustion. One can see that the zone of the hydrogen and oxygen mixing after a time of t=40 μs is formed. After the ignition (t=50 μs) a small quantity of hydrogen in the zone of mixing "burns down" and the diffusion front of combustion is forming the point of the temperature maximum. A small quantity of oxygen remains in the "zone of hydrogen".

Modeling of real burst disk rupture

(transverse shocks and turbulent mixing)

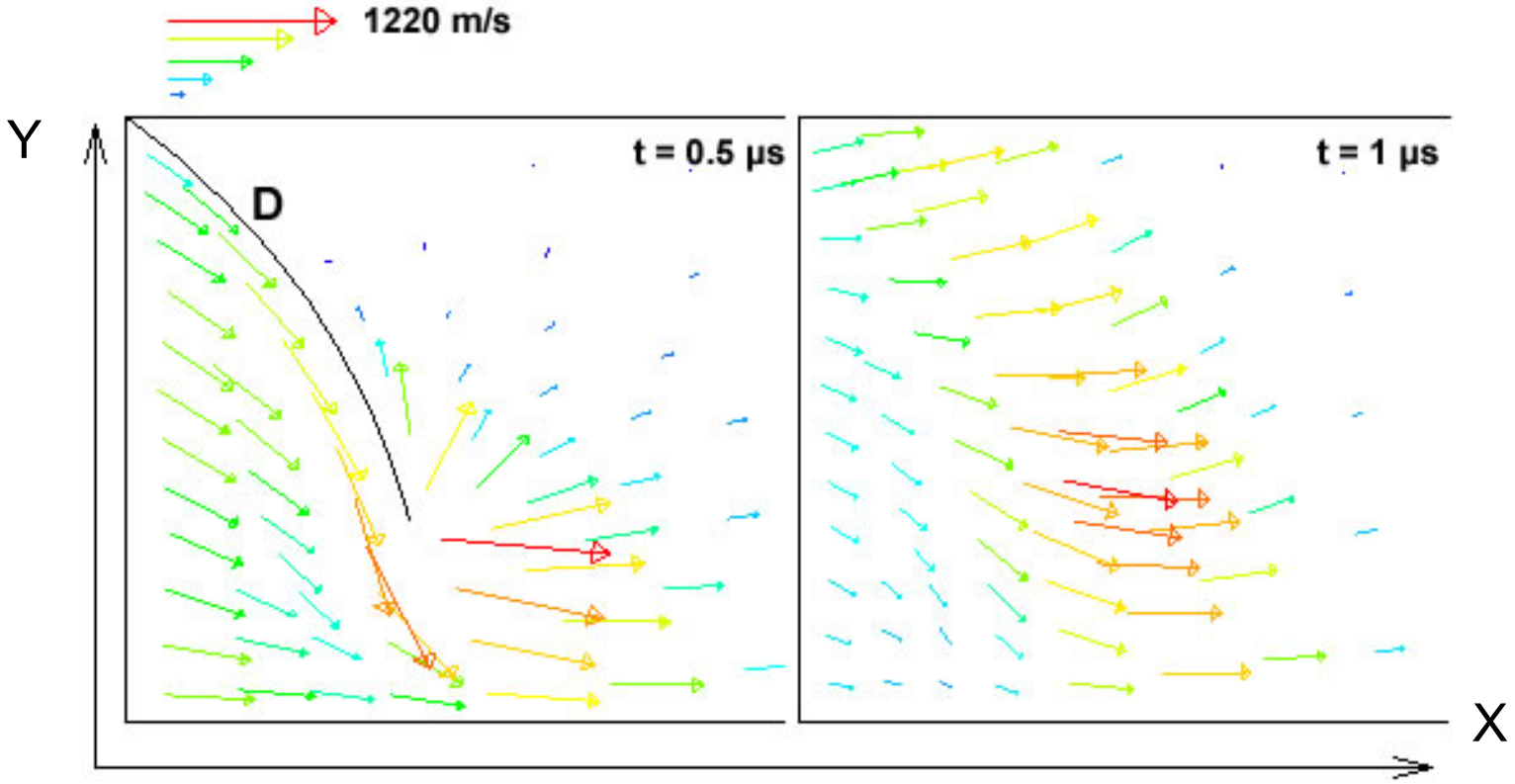

Calculated map of velocities in cylindrical tube near the "real burst disk"(D) upon discharge of hydrogen into the tube at different time moments. X – axial direction, Y – radial direction.

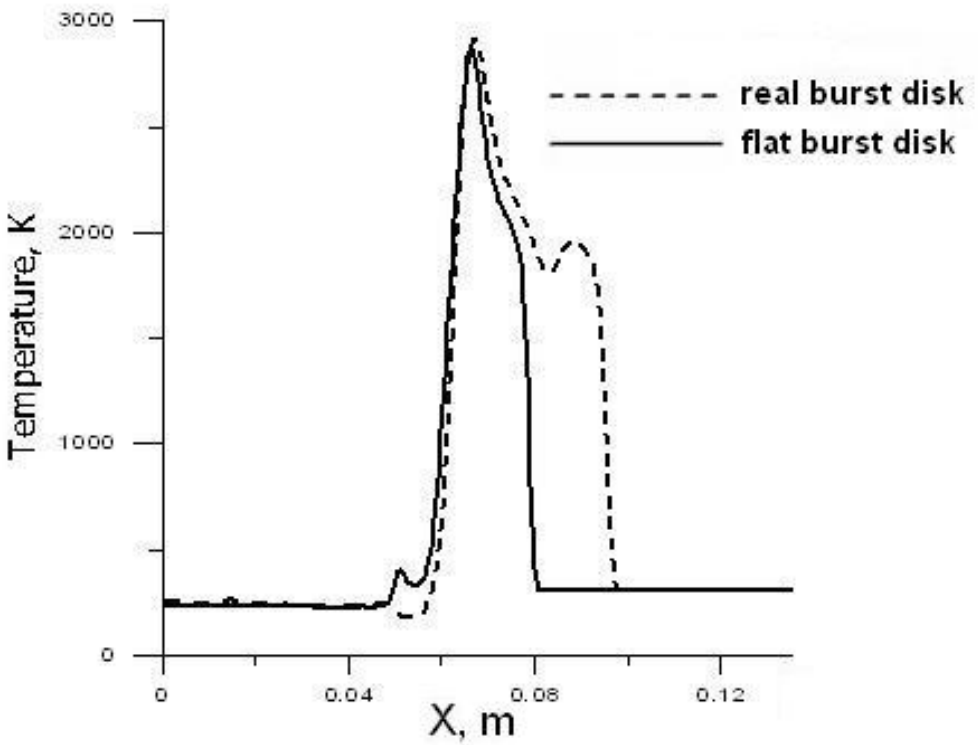

Calculated distribution of temperature on the tube wall upon the discharge through "real burst disk" and flat burst disk.

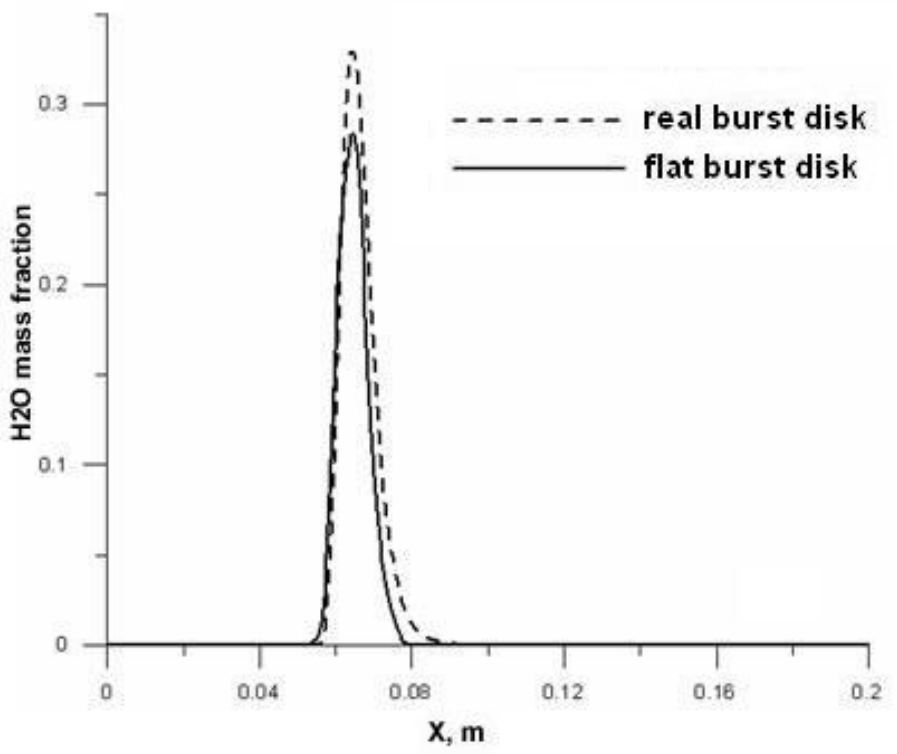

Calculated distribution of mass fraction of water vapour along the tube wall upon the discharge through "real burst disk" and flat burst disk.

Influence of boundary layer

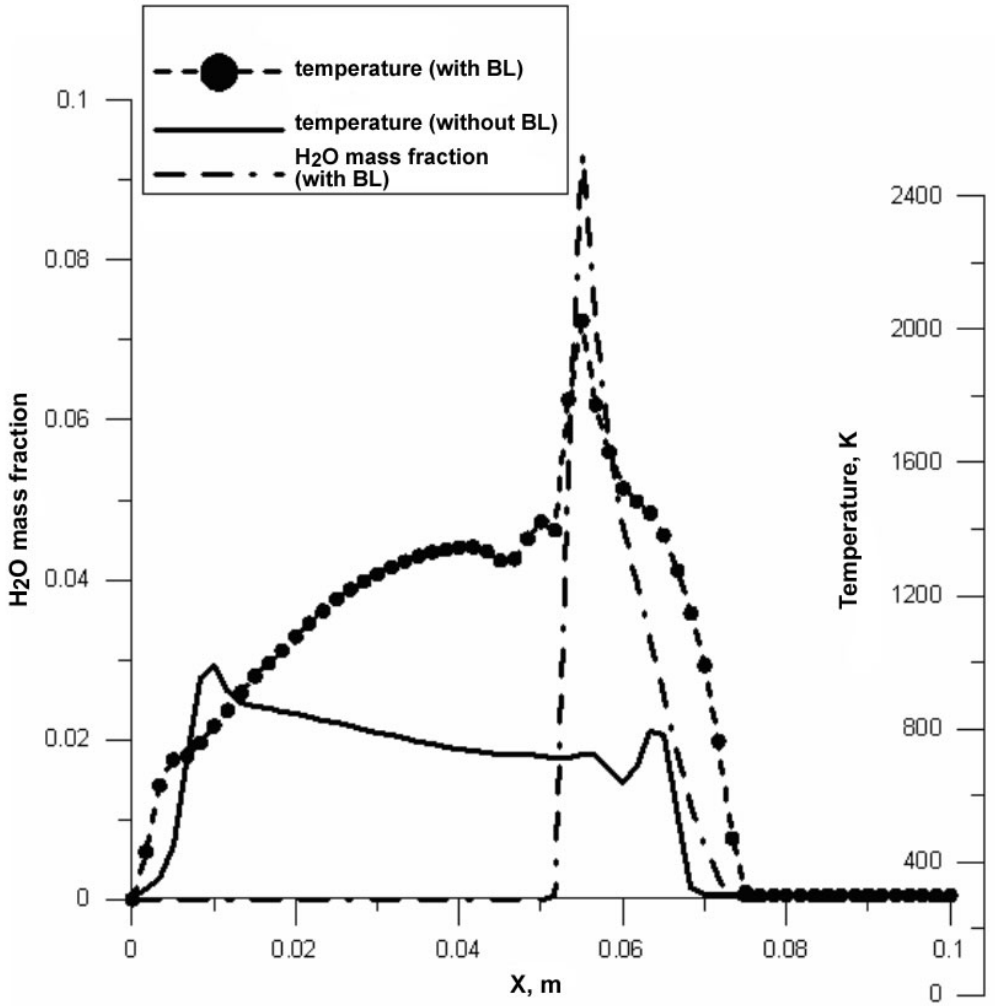

Calculated distributions of temperatures and mass fraction of water vapour on the tube wall with boundary layer and without last one (t=45 μs).

Taking into account the boundary layer the ignition occurs on the wall at hydrogen pressure less than the one without boundary layer.

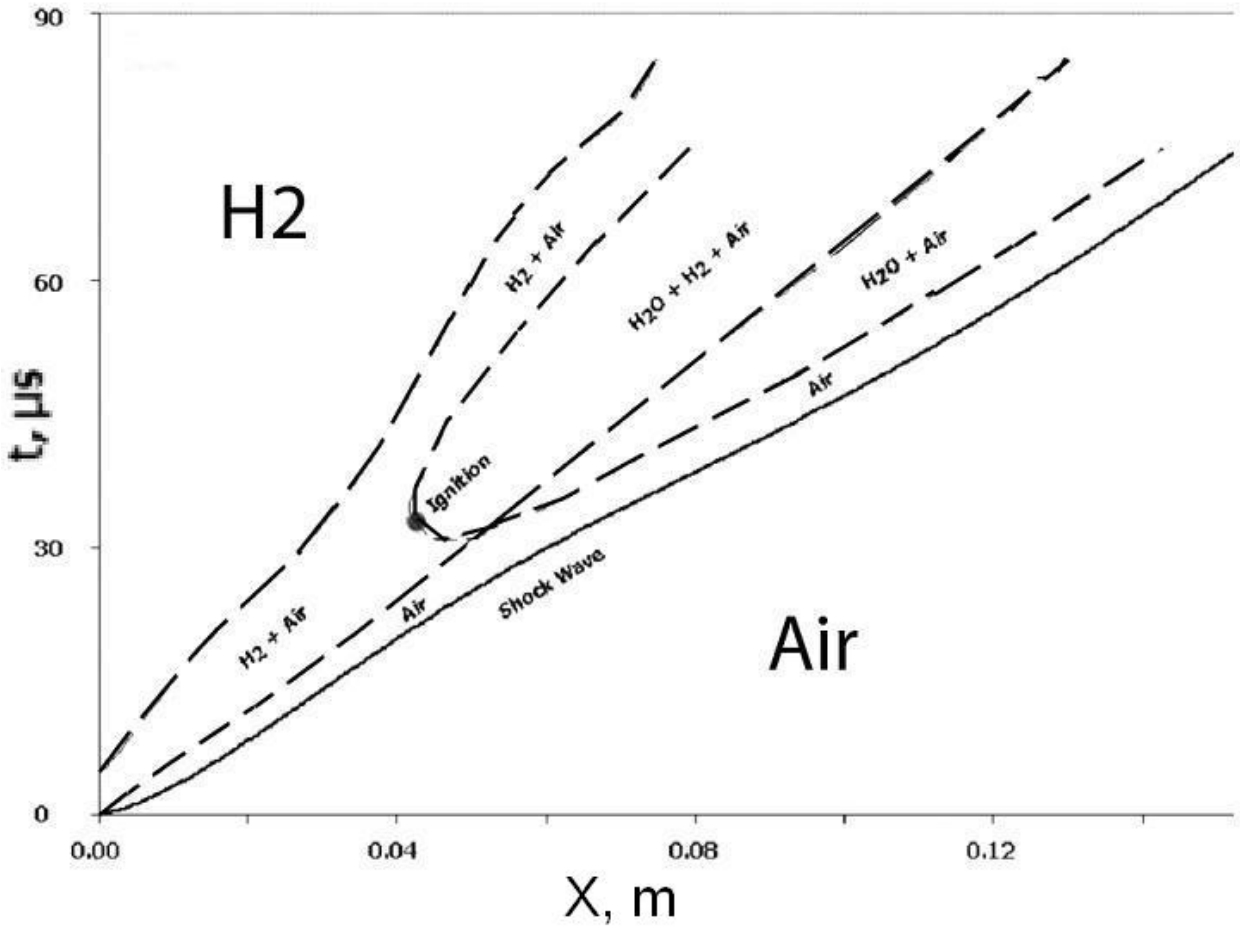

Calculated x-t diagram of trajectories of species in the tube during self-ignition of discharging hydrogen. Initial pressure of hydrogen – 80 atm.

The mixing of hydrogen with air occurs on the contact surface immediately after the burst. Mixture cloud drifts downstream along the tube. At the some moment ignition occurs. Combustion region involves fresh hydrogen and air from both sides of the burning cloud. Combustion, which being started as kinetic one, acquires diffusion character. Heat release and flame turbulence intensify mixing of reagents and such burning cloud may propagate along the tube far enough.

Comparison of experimental and numerical results

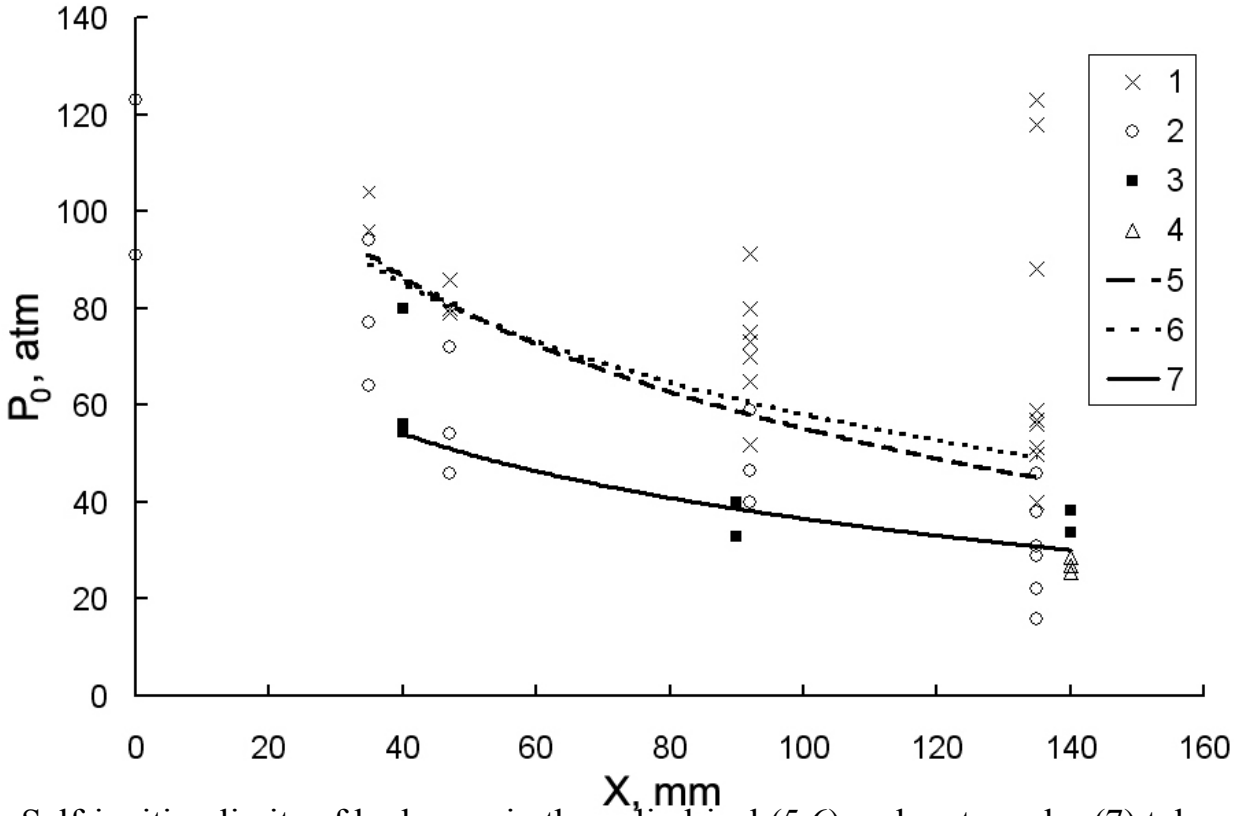

Decrease of hydrogen pressure leads to the increase of length required for the self-ignition. In rectangular tube self-ignition occurs at the pressures lower by 1.5-2 times than that in cylindrical tube.

Self-ignition limits of hydrogen in the cylindrical (5,6) and rectangular (7) tubes. X – distance from the burst disk along the axis of the tube, P_0 – initial pressure in high-pressure chamber.
1 – ignition in the cylindrical tube, experiment; 2 – no ignition in the cylindrical tube, experiment;
3 – ignition in the rectangular tube, experiment; 4 – no ignition in rectangular tube, experiment;
5 – self-ignition limit in the cylindrical tube, experiment;
6 – self-ignition limit in the cylindrical tube, numerical calculation;
7 – self-ignition limit in the rectangular tube, experiment.

Conclusions

• Hydrogen self-ignition in the tubes of round and rectangular cross section is possible at hydrogen initial pressure of 40 atm and higher.

•Experimental and numerical work has shown that increases in the initial pressure in the high-pressure chamber decreases the distance from the burst location to the hydrogen ignition point on the contact surface.

•It has been shown experimentally and numerically that at the same cross section area the self-ignition in the narrow rectangular tube occurred at lower pressure than that in cylindrical tube. At the initial pressure in high pressure chamber less on 15-20 atm self-ignition occurs at the same distance.

How to avoid combustible gas self-ignition outflowing into oxidizer medium?

Now we are working on this.
Join us!